HOKKAIDO UNIVERSITY

Title	Study on the origin of atmospheric water-soluble organic aerosols at the high-altitude observatory, Réunion island in the tropical Indian Ocean
Author(s)	Simu, Sharmine Akter
Citation	北海道大学. 博士(環境科学) 甲第14764号
Issue Date	2022-03-24
DOI	10.14943/doctoral.k14764
Doc URL	http://hdl.handle.net/2115/85774
Type	theses (doctoral)
File Information	SIMU_Akter_Sharmine.pdf

Instructions for use

Hokkaido University Collection of Scholarly and Academic Papers : HUSCAP

Study on the origin of atmospheric water-soluble organic aerosols at the high-altitude observatory, Réunion Island in the tropical Indian Ocean

（熱帯インド洋レユニオン島の高高度観測所における大気水溶性有機エアロゾルの起源に関する研究）

DISSERTATION

Sharmine Akter Simu

17 February 2022

GRADUATE SCHOOL OF ENVIRONMENTAL SCIENCE
HOKKAIDO UNIVERSITY

Acknowledgments

This thesis is the result of the three years' studies I accomplished as a Ph.D. student at the Graduate School of Environmental Science, and the Institute of Low Temperature Science, Hokkaido University. During this time, I got the opportunity to involve with many inspiring people who contributed directly or indirectly to this study. I want to thank everyone for their expert advice, support, and encouragement throughout the experimental and theoretical studies of this project.

I would particularly like to express my deepest gratitude and respect to my supervisor **Asst. Prof. Yuzo Miyazaki** for his guidance, a lot of discussion and advice, and his indefatigable eagerness in correcting my numerous mistakes. Without the manifold support he gave me, I would not have completed this thesis. He always supported me whenever I needed him to improve my research, even on weekends. I would also like to offer my special thanks to my supervisor for allowing me to study marine atmospheric aerosols in the Atmospheric Chemistry Group, his supervision during my Ph.D. course. I would like to express my deep gratitude to **Ms. Eri Tachibana** for the chemical analyses, expertise, help, and guidance.

I would like to express my gratefulness to all the faculty members of biogeochemistry course, who always give me suggestions and insights of thoughts. I also owe my deepest gratitude to the **committee members of the Graduate School of Environmental Science** for their understanding and support, who enabled me to pass my pre-defense and defense despite of difficult circumstances. Throughout the Ph.D. journey, I learned many new things from them, especially from **Prof. Yoshito Chikaraishi,** who is always supportive and provided me positive motivation by his nice words. I also acknowledge **Prof. Koji Suzuki**, **Assoc. Prof. Sohiko Kameyama**, and **Assoc. Prof. Yoko Iwamoto** (the Graduate School of Integrated Sciences for Life, Hiroshima University) for

their extraordinary supports as reviewers and for helpful comments and suggestions for my thesis. I am grateful to **Tsukasa Dobashi,** for helping me in data analysis and even in other problems.

I would like to express my gratitude to the **OCTAVE** (Oxygenated Compounds in the Tropical Atmosphere: Variability and Exchanges) team for giving me the opportunity to conduct my Ph.D. as a part of the project. It is really a privilege for me to be a part of such a big project with all the great scientists. I would like to thank **Jean-Marc Metzger** for deploying the aerosol samplers in the Reunion Island. I also want to give thanks to **Jérôme Brioude, Rainer Volkamer**, and **Trissevgeni Stavrakou** who coordinated the project and aerosol samplings at the research sites. I am grateful to **Henning Finkenzeller**, **Jérôme Brioude, Aurélie Colomb,** and **Olivier Magand** for their help in the aerosol samplings. I am very much grateful to **Bert Verreyken, Stephanie Evan**, and **Jérôme Brioude** for performing FLEXPART simulations in the research. I also thank my friend **Nur Hussain** and **Mustafizur Rahman** for their help in making the global and regional map of marine primary productivity, respectively.

I would like to thank the scholarship "Special Grant Program for International Students", the **Ministry of Education, Culture, Sports, Science and Technology (MEXT)** in Japan. Without its financial support, this thesis would be impossible. I also want to acknowledge **OPAR** (Observatoire de Physique de l'Atmosphère à La Réunion) which is funded by **CNRS- INSU** and Université de La Réunion and managed by **OSU-R** (Observatoire des Sciences de l'Univers à La Réunion, UMS 3365). I want to thank everyone who had a part in this work and whom I did not mention here by name. I humbly ask for their indulgence.

Thanks, is also given to my **friends** who accompanied me during the past years of this thesis, and my **family** for the encouragements. Particularly, I like to express my deepest gratitude to my **parents** for their continuous support and for their trust in me and my abilities to achieve my goals.

During my Ph.D. course, I lost my father due to COVID-19, and I could not support him in his last days. It is an unrecoverable loss in my life. I wish he would be with me when I achieve my degree.

And finally, I especially thank my partner **Mr. Abul Kashem** for his love, support, and patience during the past years. I'm grateful to our daughter **Nabeeha Noor Aleena** who gave me the motivation and energy to complete the thesis. I want to dedicate my Ph.D. degree to my daughter **Nabeeha Noor Aleena** for sacrificing her childhood memories with her mother and I also sacrificed my motherhood for this degree. I am delighted that her sacrifice is going to be successful finally, and she deserves this dedication.

Abstract

The ocean is a major source of submicrometer aerosols, that play an important role in the atmospheric radiative budget because they determine the number of cloud condensation nuclei (CCN) and ice nuclei (IN). Marine-derived submicrometer organic aerosols (OAs) potentially can affect the marine aerosol optical depth (AOD) as well as CCN and IN concentrations. These are particularly important over remote oceans, as these areas experience minimal influence from anthropogenic emissions originating from terrestrial sources. The tropical Indian Ocean (IO) is expected to be a significant source of water-soluble organic aerosols (WSOAs) that are important factors relevant to the cloud formation of aerosol particles, because of high marine primary productivity in this oceanic region. Current atmospheric numerical models significantly underestimate the budget of organic aerosols and their precursors, especially over the tropical oceans. This is primarily due to poor knowledge of sources and paucity of observations on these parameters regarding spatial and temporal variation over the tropical open ocean.

To evaluate the contribution of sources to WSOA as well as their formation processes, submicrometer aerosol sampling was conducted at the high-altitude Maïdo observatory (21.1°S, 55.4°E, 2,160 m a.s.l), located on the remote island of La Réunion in the southwest IO. The sampling was made within the framework of an international project, OCTAVE (Oxygenated Compounds in the Tropical Atmosphere: Variability and Exchanges). The aerosol samples were continuously collected during local daytime and nighttime, which corresponded to the ambient conditions of the marine boundary layer (MBL) and free troposphere (FT), respectively, from March 15 to May 24, 2018.

The water vapor mixing ratio and their seasonal changes confirm that the observatory was located in the MBL during daytime and in the FT at night. The wet season is characterized by

higher marine primary productivity and atmospheric relative humidity than in the dry season. Moreover, vertical transport of air from the ocean surface was more active due to the synoptic-scale meteorology. In MBL, the OC concentrations during the wet season were generally higher than those during the dry season, which likely reflects higher marine primary productivity. The temporal trends of OC and WSOC suggest that the water-soluble fraction of OC was an important factor controlling the total organic matter in the submicrometer aerosols during the wet season.

Chemical analysis showed that organic matter was the dominant component of submicrometer water-soluble aerosol (~45 ± 17%) during the wet season (March 15–April 23). On the other hand, sulfate dominated (~77 ± 17%) during the dry season (April 24–May 24), most of which was attributable to the effect of a volcanic eruption. Measurements of the stable carbon isotope ratios of water-soluble organic carbon (WSOC) suggested that marine sources contributed significantly (~70%) to the observed WSOC mass in both the MBL and the FT in the wet season, whereas a mixture of marine and terrestrial sources dominantly contributed to WSOC in the dry season. The distinct seasonal changes in the dominant source of WSOC were also supported by Lagrangian trajectory analysis.

Positive matrix factorization analysis suggested that marine secondary OA dominantly contributed to the observed WSOC mass (~70%) during the wet season, whereas mixtures of marine and terrestrial sources contributed during the dry season in both MBL and FT. Overall, this study demonstrates that secondary formation of marine-derived aerosol is likely important up to the FT in the wet season, when marine biological activity and vertical transport are more significant. The formation of marine secondary OA is a process generally missing in current climate models. Current models typically consider only marine primary OA (i.e., sea spray aerosols) from the sea surface to represent the OA burden in tropical “pristine” oceanic regions. The impacts of marine

secondary OA up to FT aerosols lead to changes in the microphysical and optical properties of aerosol particles. The findings in this study can lead to a better understanding of the climate effects of aerosols in these oceanic regions.

Table of Contents

List of publications

Simu, S. A., Miyazaki, Y., Tachibana, E., Finkenzeller, H., Brioude, J., Colomb, A., Magand, O., Verreyken, B., Evan, S., Volkamer, R., and Stavrakou, T.: Origin of water-soluble organic aerosols at the Maïdo high-altitude observatory, Réunion Island in the tropical Indian Ocean, *Atmos. Chem. Phys.*, 21(22), 17017–17029, https://doi.org/10.5194/acp-21-17017-2021, 2021

Abbreviations

AOD	aerosol optical depth
ARE	aerosol radiative effect
CCN	cloud condensation nuclei
CDNC	cloud droplet number concentration
DMS	dimethyl sulfide
ECMWF	European Centre for Medium-Range Weather Forecasts
FT	free troposphere
IN	ice nuclei
IO	the Indian Ocean
LOD	limit of detection
MBL	marine boundary layer
MSA	methanesulfonic acid
OA	organic aerosol
OC	organic carbon
OCTAVE	Oxygenated Compounds in the Tropical Atmosphere: Variability and Exchanges
PMF	positive matrix factorization
POA	primary organic aerosol
SS	sea salt

SSAs	sea spray aerosols
SOA	secondary organic aerosol
TMS	trimethylsilyl
VOCs	volatile organic compounds
VPDB	Vienna Pee Dee Belemnite
WIOC	water-insoluble organic carbon
WSOA	water-soluble organic aerosol
WSOC	water-soluble organic carbon
3-MBTCA	3-methyl-1,2,3-butanetricarboxylic acid

Chapter 1. General Introduction

1.1 Marine atmospheric aerosols and their impact on climate

The ocean covers about 70% of the Earth's surface and acts as a major source of atmospheric aerosols, which play a key role in controlling the atmospheric radiative forcing. Aerosols can affect the radiative forcing directly by absorbing and scattering radiation and indirectly by acting as cloud condensation nuclei (CCN) or ice nuclei (IN) to form cloud particles. The latter effect leads to changes in the albedo (and thus ambient temperature) and in the amount of precipitation (Twomey, 1974; Albrecht, 1989).

Figure 1.1 illustrates the general formation mechanism of marine atmospheric aerosols and their impact on the climate. There are two major processes of aerosol formation from the ocean. One is the primary emission of marine aerosols which is the direct emission of sea spray aerosols (SSAs). By the bubble bursting process, SSAs are emitted from the sea surface to the atmosphere. SSAs are known to have a complex mixture of sea salt (SS) and an array of organic species with differing water solubility (Parungo et al., 1986; Blanchard, 1989; Leck and Bigg, 2005). The other process is a secondary formation of aerosols, which is derived from the oxidation of precursors such as volatile organic compounds (VOCs), including dimethyl sulfide (DMS). VOCs emitted from the ocean surface are reacted to subsequently form secondary organic aerosols (SOA) in the atmosphere.

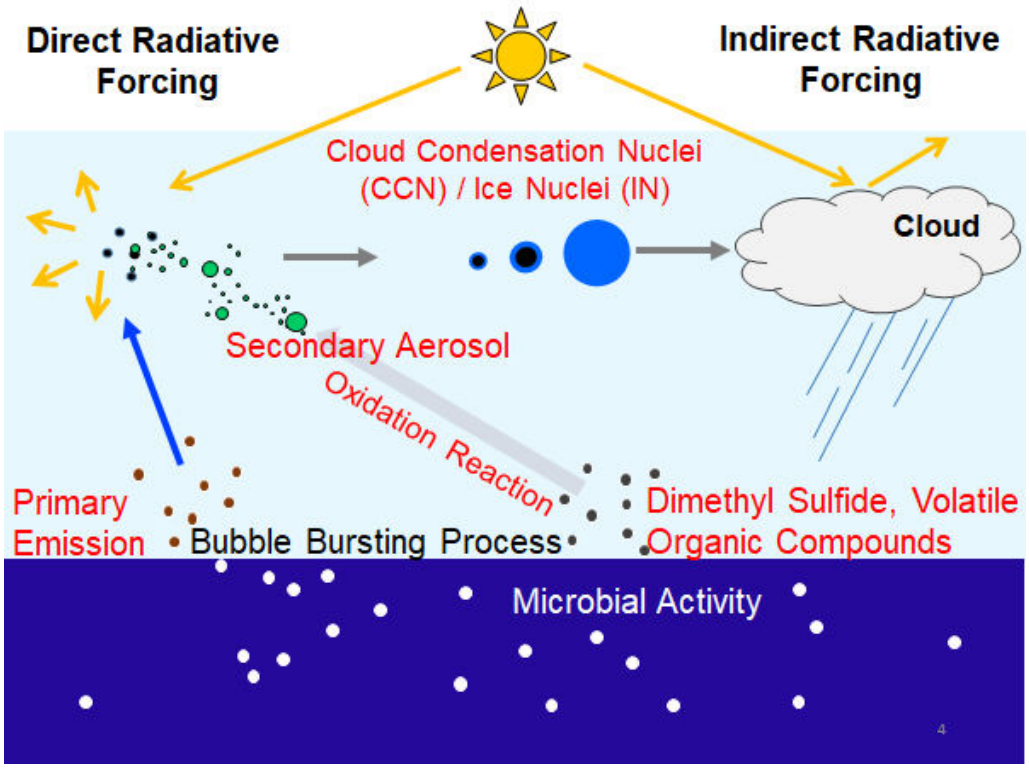

Figure 1.1 Schematic of chemical components and formation processes of marine submicrometer aerosols and their impact on climate.

Figure 1.2 shows an example of the radiative forcing of aerosols by direct and indirect effects. In addition to "classical" indirect effects of aerosols (cloud albedo), Mahowald (2011) proposed indirect effects by biogeochemical cycles, which were estimated to be comparable to the direct and indirect effects via cloud albedo. However, large uncertainty exists in these radiative forcing.

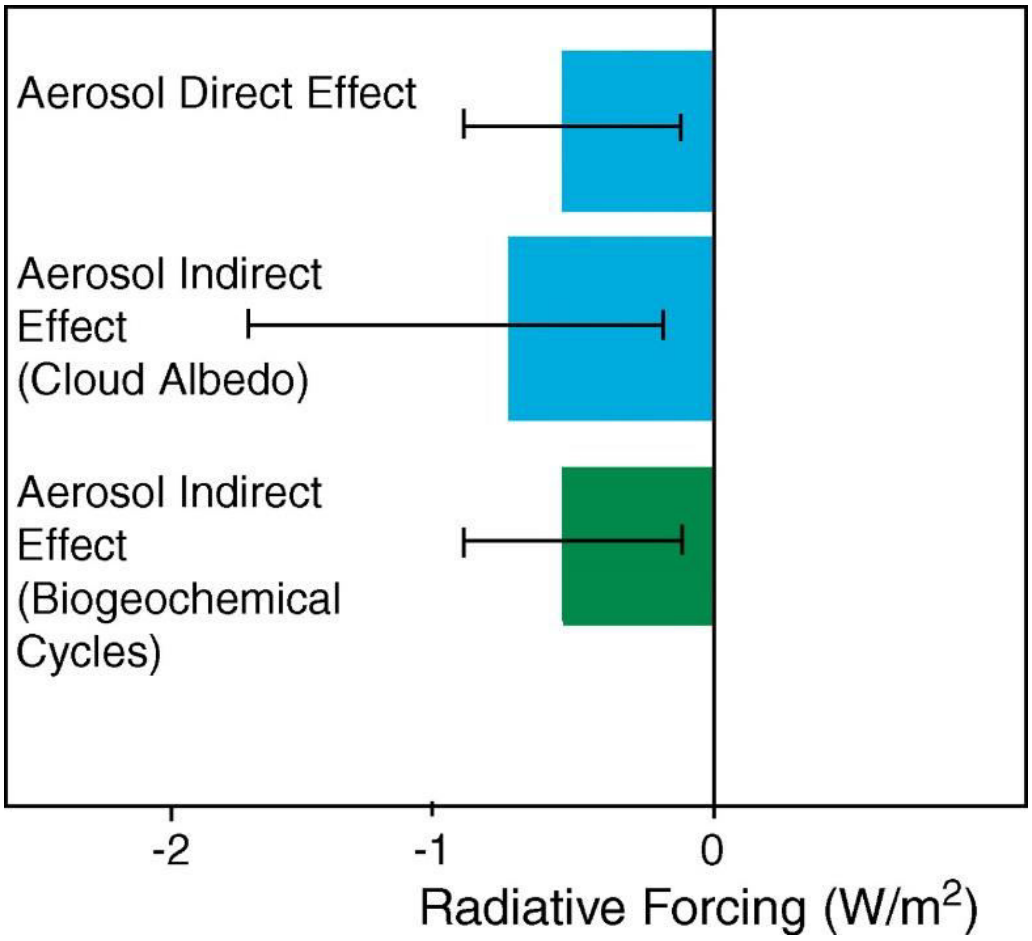

Figure 1.2 Radiative forcing (W/m^2) of aerosol direct and indirect (cloud albedo and biogeochemical cycles) effects with error bars showing each uncertainty (Mahowald 2011).

1.2 Important parameters of aerosols for climate effects

There are several important parameters of aerosol particles for climate effects, which include (1) particle size, (2) chemical composition, and (3) water-solubility of aerosol particles along with the formation process. Particle size can be classified into submicrometer aerosols (< 1 μm in diameter) and supermicrometer aerosols (> 1 μm in diameter). The residence time of submicromter aerosols in the atmosphere is approximately one week, whereas supermicrometer aerosols can

reside in the atmosphere on timescales of hours to a day. Submicrometer aerosols can be more suitable to act as CCN to form clouds.

Regarding chemical composition, sulfate and organic matter as well as the other sea salt components have been known as major species in marine atmospheric aerosols. Sulfate in marine aerosols is mainly formed by the oxidation of organosulfur gases, principally DMS emitted from the ocean surface (Fitzgerald, 1991). It has been known that sulfate is highly hygroscopic, which has a high ability to act as CCN. Organic matter typically dominates submicrometer aerosols, which can both promote and suppress the CCN activity depending on its composition.

Water-solubility of aerosol particle is also an important factor to act as CCN to form clouds. Water-soluble organic aerosols in the marine atmosphere can be formed by both primary emission and secondary formation. Novakov and Penner (1993) indicated that 37% of the CCN number-concentration measured at a marine site could be accounted for using total sulfate particles, while the remaining 63% were attributed to organic aerosols. In some cases, the concentration of water-soluble organics is positively correlated with the number of CCN (Sun and Ariya, 2006).

1.3 Tropical Indian Ocean as potential sources of water-soluble organic aerosols

Tropical oceans cover a large area of the global ocean surface. Approximately 30% of the world's areas are occupied by tropical oceans (Pidwirny, 2006). Tropical environments have a unique climate in terms of the higher temperatures and, in particular, the patterns of rainfall and humidity (Payne and Edis, 2012). For these reasons, the tropical ocean is rich in biodiversity due to favorable environmental conditions. As shown in **Figure 1.3**, The tropical Indian Ocean (IO) is

an oceanic region with high primary productivity (Jayaraman et al., 1998; Langley DeWitt et al., 2013; Höpner et al., 2016).

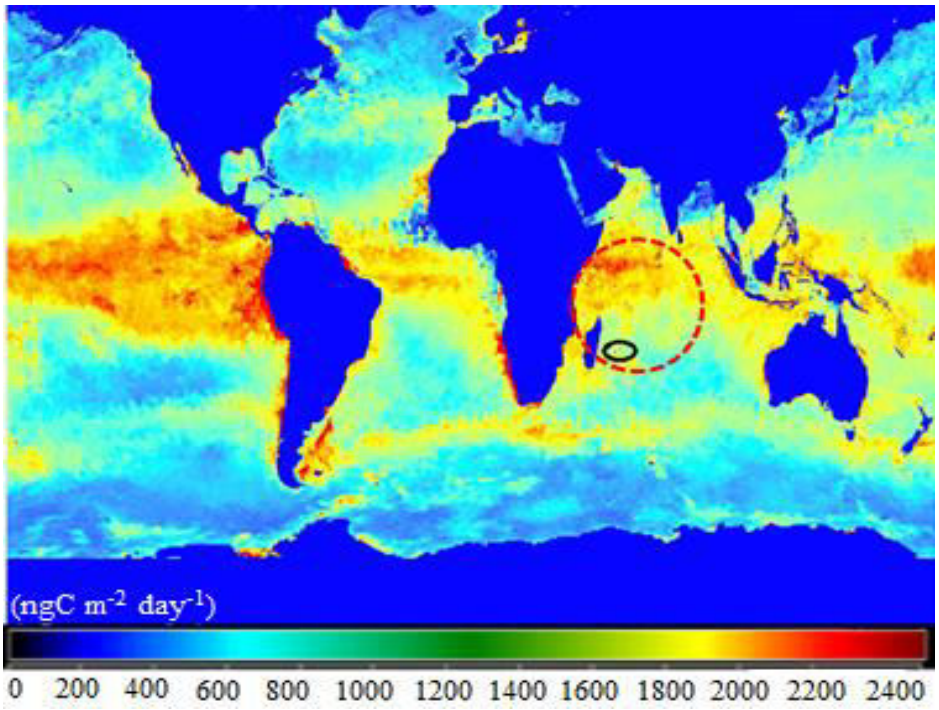

Figure 1.3 Annual average of marine primary productivity for the year 2018.The colors in the map explain the productivity condition of the ocean. The blue (0–1200 ngC $m^{-2}day^{-1}$), green (1200–1800 ngC $m^{-2}day^{-1}$) and from yellow to red (1800–2400 ngC $m^{-2}day^{-1}$) colors indicate oligotrophic, mesotrophic, and eutrophic states of the oceanic regions, respectively (Carr et al., 2006; Istvánovics, 2009). The red dashed circle indicates a region of Indian Ocean with high primary productivity, and the black circle indicates the location of the Maïdo high-altitude observatory. The figure was produced and adapted from the NASA's OceanColor Web (http://oceancolor.gsfc.nasa.gov/cgi/l3, last access: 7 July 2021).

High marine primary productivity is expected to provide huge sources of organic aerosols (Jayaraman et al., 1998; Langley Dewitt et al., 2013; Höpner et al., 2016) as well as significant

emissions of VOCs, including oxygenated VOCs. Ocean-derived sub-micrometer particles contain a large fraction of water-soluble organic carbon (WSOC) as well as water-insoluble organic carbon (WIOC) (O'Dowd et al., 2004; Prather et al., 2013; Miyazaki et al., 2018). Cloud droplet number concentration (CDNC) over the remote oceans ranges from a few tens per cm^3 in biologically inactive regions (seasons) to a few hundred per cm^3 under biologically active conditions (Andreae, 2007).

A number of studies have focused on aerosols over the northern IO, particularly around India (Chylek et al., 2006; Madhavan et al., 2008; Srinivas and Sarin, 2013). These studies mainly focused on the impact of anthropogenic contribution and land influences from different sources of aerosols over the northern IO, especially from the Asia region. The southern IO is one of the few pristine regions in the global ocean. Pristine oceanic regions are important to estimate the contribution of natural oceanic sources to aerosol burden as those regions are less affected by anthropogenic sources. However, there are little data on organic aerosols over this pristine oceanic region. Large uncertainties exist in the amount and relative importance of primary emission and secondary formation of organic aerosols in the tropical IO. As a result, the contribution of marine organic aerosol to the radiative balance of the atmosphere is still highly uncertain.

1.4 Importance of vertical distributions of aerosols

The marine boundary layer (MBL) is the part of the atmosphere closest to the marine surface and thereby is directly influenced by the marine–atmosphere exchanges of aerosols, moisture, energy, sea salts, trace gases and VOCs (Díaz et al., 2019). The layer above the MBL is termed as free troposphere (FT) where the interaction between the ocean surface and the atmosphere is less significant. MBL and FT act as a pivotal role in the climate for realistic modeling of cloud

properties (Díaz et al., 2019) by regulating the vertical exchange of different components between the ocean surface and FT (Zhang et al., 2018), plays a key role in controlling entrainment efficiency, energy and mass fluxes, cloud formation processes, etc. (Díaz et al., 2019), which lead to changes in the surrounding temperature, humidity, turbulence, wind, and so on (Chan and Wood, 2013).

Aerosols at different altitudes have different physical and optical properties depending on their size (Pappas et al., 2015). The growth of nucleation and Aitken aerosols in the MBL represents a substantial source of accumulation-mode aerosols with the highest contribution potentially reaching 60% in the Northeast Atlantic in summer (Zheng et al., 2018; Wang et al., 2021). Vertical distribution of aerosols impacts the aerosol radiative effect (ARE) (Mishra et al., 2015). The sensitivity of the aerosol forcing to the vertical distribution of aerosols depends on the presence of clouds, surface albedo and aerosol properties (Haywood and Shine, 1997; Choi and Chung, 2014). Low and high-altitude aerosols play an important role forming distinct cloud droplets. Previous studies showed that the overall impact of high-altitude clouds is to warm the planet, whereas low-altitude clouds are supposed to cool down, which is essential to change albedo effects.

Table 1.1 summarizes the advantages and disadvantages of various tools for aerosol measurements including vertical observation. For example, aircraft measurement can cover both horizontal and vertical distributions of aerosol parameters, but it is difficult to obtain continuous time-series data at certain locations. Mountain site observatories are suitable for obtaining time-series data with a number of parameters for aerosols. So far, there is no study on the origin of organic aerosols measured under MBL and FT conditions over the pristine IO environments.

Table 1.1 Tools of aerosol measurement and their comparison considering different parameters. The symbols indicate advantages or disadvantages for each aerosol measurement tool.

	Aircraft	Satellite	Ship	Ground	Mountain site
Spatial coverage (horizontal)	○	◎	○	×	×
Spatial coverage (vertical)	○	○	△	△	△
Time series	×	○	△	◎	◎
The number of parameters	○	△	◎	◎	◎

1.5 Objectives of the study

This study aims to evaluate the contribution of marine or terrestrial sources to water-soluble organic aerosols and their formation processes in MBL and FT over the tropical IO. To achieve this, submicrometer aerosol samples obtained at the high-altitude Maïdo observatory, located on the remote island of La Réunion in the southwest IO, were analyzed to derive aerosol chemical parameters, including stable carbon isotope ratios. The discussion is based on the time-series data in day and nighttime, representing aerosols under the MBL and FT conditions. Moreover, seasonal changes in the origin of WSOC are investigated in this thesis.

References

Albrecht, B.: Aerosols, cloud microphysics, and fractional cloudiness, Science, 245, 1227–1230, https://doi.org/10.1126/science.245.4923.1227, 1989a.

Andreae, M. O.:Aerosols before pollution, Science, 315, 50–51, https://doi.org/10.1126/science.1136529, 2007.

Blanchard, D. C.: The ejection of drops from the sea and their enrichment with bacteria and other materials: A review, Estuaries, 12, 127–137, https://doi.org/10.2307/1351816, 1989.

Carr, M. E., Friedrichs, M. A. M., Schmeltz, M., Noguchi Aita, M., Antoine, D., Arrigo, K. R., Asanuma, I., Aumont, O., Barber, R., Behrenfeld, M., Bidigare, R., Buitenhuis, E. T., Campbell, J., Ciotti, A., Dierssen, H., Dowell, M., Dunne, J., Esaias, W., Gentili, B., Gregg, W., Groom, S., Hoepffner, N., Ishizaka, J., Kameda, T., Le Quéré, C., Lohrenz, S., Marra, J., Mélin, F., Moore, K., Morel, A., Reddy, T. E., Ryan, J., Scardi, M., Smyth, T., Turpie, K., Tilstone, G., Waters, K. and Yamanaka, Y.: A comparison of global estimates of marine primary production from ocean color, Deep-Sea Res. Pt. II, 53, 741–770, https://doi.org/10.1016/j.dsr2.2006.01.028, 2006.

Chan, K. M. and Wood, R.: The seasonal cycle of planetary boundary layer depth determined using COSMIC radio occultation data, J. Geophys. Res.-Atmos., 118, 12,422-12,434, https://doi.org/10.1002/2013JD020147, 2013.

Choi, J. O. and Chung, C. E.: Sensitivity of aerosol direct radiative forcing to aerosol vertical profile, e, Tellus B: Chemical and Physical Meteorology, 66, 24376, https://doi.org/10.3402/tellusb.v66.24376, 2014.

Chylek, P., Dubey, M. K., Lohmann, U., Ramanathan, V., Kaufman, Y. J., Lesins, G., Hudson, J., Altmann, G. and Olsen, S.: Aerosol indirect effect over the Indian Ocean, Geophys. Res.

Lett., 33, 2–5, https://doi.org/10.1029/2005GL025397, 2006.

Díaz, J. P., Expósito, F. J., Pérez, J. C., González, A., Wang, Y., Haimberger, L. and Wang, J.: Long-term trends in marine boundary layer properties over the Atlantic Ocean, J. Clim., 32, 2991–3004, https://doi.org/10.1175/JCLI-D-18-0219.1, 2019.

Fitzgerald, J. W.: Marine aerosols: A review, Atmos. Environ. Part A, Gen. Top., 25, 533–545, https://doi.org/10.1016/0960-1686(91)90050-H, 1991.

Haywood, J. M. and Shine, K. P.: Multi-spectral calculations of the direct radiative forcing of tropospheric sulphate and soot aerosols using a column model, Q. J. R. Meteorol. Soc., 123, 1907–1930, https://doi.org/10.1256/smsqj.54306, 1997.

Höpner, F., A.-M. Bender, F., Ekman, A. M. L., Praveen, P. S., Bosch, C., Ogren, J. A., Andersson, A., Ogren, J. A. and Ramanathan, V.: Vertical profiles of optical and microphysical particle properties above the northern Indian Ocean during CARDEX 2012, Atmos. Chem. Phys., 16, 1045–1064, https://doi.org/10.5194/acp-16-1045-2016, 2016.

Istvánovics, V.: Eutrophication of Lakes and Reservoirs, Encycl. Inl. Waters, 157–165, https://doi.org/10.1016/B978-012370626-3.00141-1, 2009.

Jayaraman, A., Lubin, D., Ramachandran, S., Ramanathan, V., Woodbridge, E., W. D. Collins, and K. S. Zalpuri: Direct observations of aerosol radiative forcing over the tropical Indian Ocean during the January-February 1996 pre-INDOEX cruise, J. Geophys. Res., 103, 827–836, 1998.

Langley DeWitt, H., Coffman, D. J., Schulz, K. J., Alan Brewer, W., Bates, T. S. and Quinn, P. K.: Atmospheric aerosol properties over the equatorial Indian Ocean and the impact of the Madden-Julian Oscillation, J. Geophys. Res.-Atmos., 118, 5736–5749, https://doi.org/10.1002/jgrd.50419, 2013.

Leck, C. and Bigg, E. K.: Biogenic particles in the surface microlayer and overlaying atmosphere in the central Arctic Ocean during summer, Tellus B: Chemical and Physical Meteorology, 57, 305–316, https://doi.org/10.3402/tellusb.v57i4.16546, 2005.

Madhavan, B. L., Niranjan, K., Sreekanth, V., Sarin, M. M. and Sudheer, A. K.: Aerosol characterization during the summer monsoon period over a tropical coastal Indian station, Visakhapatnam, J. Geophys. Res.-Atmos.,113, 1–16, https://doi.org/10.1029/2008JD010272, 2008.

Mahowald, N.: Aerosol indirect effect on biogeochemical cycles and climate, Science, 334, 794–796, https://doi.org/10.1126/science.1207374, 2011.

Mishra, A. K., Koren, I. and Rudich, Y.: Effect of aerosol vertical distribution on aerosol-radiation interaction: A theoretical prospect, Heliyon, 1, https://doi.org/10.1016/j.heliyon.2015.e00036, 2015.

Miyazaki, Y., Yamashita, Y., Kawana, K., Tachibana, E., Kagami, S., Mochida, M., Suzuki, K. and Nishioka, J.: Chemical transfer of dissolved organic matter from surface seawater to sea spray water-soluble organic aerosol in the marine atmosphere, Sci. Rep., 8, 1–10, https://doi.org/10.1038/s41598-018-32864-7, 2018.

Novakov, T. and Penner, J. E.: Large contribution of organic aerosols to cloud-condensation-nuclei concentrations, Nature, 365, 823–826, https://doi.org/10.1038/365823a0, 1993.

O'Dowd, C. D. and De Leeuw, G.: "Marine aerosol production: A review of the current Knowledge, Philos. Trans. R. Soc. A, 365, 1753-1774, https://doi.org/10.1098/rsta.2007.2043, 2007

Pappas, V., Hatzianastassiou, N., Matsoukas, C., Koras Carracca, M., Kinne, S. and Vardavas, I.: Impact of aerosol vertical distribution on aerosol direct radiative effect and heating rate in the

Mediterranean region, Geophysical Research Abstracts, 17, https://meetingorganizer.copernicus.org/EGU2015/EGU2015-14669.pdf, 2015.

Parungo, F. P., Nagamoto, C. T., Rosinski, J. and Haagenson, P. L.: A study of marine aerosols over the Pacific Ocean, J. Atmos. Chem., 4, 199–226, https://doi.org/10.1007/BF00052001, 1986.

Payne, T. E. and Edis, R.: Mobility of radionuclides in tropical soils and groundwater, Radioactivity in the Environment, 18, 93–120, https://doi.org/10.1016/B978-0-08-045016-2.00003-5, 2012.

Pidwirny, M.: Introduction to the Oceans, Fundamentals of physical geography, 2nd Edition, Chapter 8, http://www.physicalgeography.net/fundamentals/ 8o.html, 2006.

Prather, K. A., Bertram, T. H., Grassian, V. H., Deane, G. B., Stokes, M. D., DeMott, P. J., Aluwihare, L. I., Palenik, B. P., Azam, F., Seinfeld, J. H., Moffet, R. C., Molina, M. J., Cappa, C. D., Geiger, F. M., Roberts, G. C., Russell, L. M., Ault, A. P., Baltrusaitis, J., Collins, D. B., Corrigan, C. E., Cuadra-Rodriguez, L. A., Ebben, C. J., Forestieri, S. D., Guasco, T. L., Hersey, S. P., Kim, M. J., Lambert, W. F., Modini, R. L., Mui, W., Pedler, B. E., Ruppel, M. J., Ryder, O. S., Schoepp, N. G., Sullivan, R. C. and Zhao, D.: Bringing the ocean into the laboratory to probe the chemical complexity of sea spray aerosol, Proc. Natl. Acad. Sci. U. S. A., 110, 7550–7555, https://doi.org/10.1073/pnas.1300262110, 2013.

Srinivas, B. and Sarin, M. M.: Light absorbing organic aerosols (brown carbon) over the tropical Indian Ocean: Impact of biomass burning emissions, Environ. Res. Lett., 8, 044042, https://doi.org/10.1088/1748-9326/8/4/044042, 2013.

Sun, J. and Ariya, P. A.: Atmospheric organic and bio-aerosols as cloud condensation nuclei (CCN): A review, Atmos. Environ., 40, 795–820,

https://doi.org/10.1016/j.atmosenv.2005.05.052, 2006.

Twomey, S.: Pollution and the planetary albedo, Atmos. Environ., 8, 1251–1256, https://doi.org/10.1016/0004-6981(74)90004-3, 1974

Wang, Y., Zheng, G., Jensen, M. P., Knopf, D. A., Laskin, A., Alyssa, A., Mechem, D., Mei, F., Moffet, R., Sedlacek, A. J., Shilling, J. E., Sullivan, A., Tomlinson, J., Veghte, D., Weber, R., Wood, R., Zawadowicz, A. and Wang, J.: Vertical profiles of trace gas and aerosol properties over the Eastern North Atlantic : Variations with season and synoptic condition, Atmos. Chem. Phys. Discuss., (April), 1–39, https://doi.org/10.5194/acp-2021-300, 2021.

Zhang, H., Zhou, X., Zou, J., Wang, W., Xue, L. and Ding, Q.: A Review on the methods for observing the substance and energy exchange between atmosphere boundary layer and free troposphere, 9, 460, https://doi.org/10.3390/atmos9120460, 2018.

Zheng, G., Wang, Y., Aiken, A. C., Gallo, F., Jensen, M. P., Kollias, P., Kuang, C., Luke, E., Springston, S., Uin, J., Wood, R. and Wang, J.: Marine boundary layer aerosol in the eastern North Atlantic: Seasonal variations and key controlling processes, Atmos. Chem. Phys., 18, 17615–17635, https://doi.org/10.5194/acp-18-17615-2018, 2018.

Chapter 2: Experimental Method

2.1 The high-altitude Maïdo observatory

The high-altitude Maïdo observatory (21.1°S, 55.4°E, 2,160 m a.s.l) is located on the remote island of La Réunion in the southwest IO (Baray et al., 2013) (**Figure 2.1**). The observatory is affected by prevailing southeasterly trade winds in the MBL. The meteorological field in that region is characterized by wet (typically from November to April) and dry seasons (from May to October). Cyclones generally occur between November and May (Baray et al., 2013) in the Indian ocean. Marine and coastal air reach the observatory during the late morning until noontime by vertical air mass movement. During the nighttime, free tropospheric air subsided on the observatory.

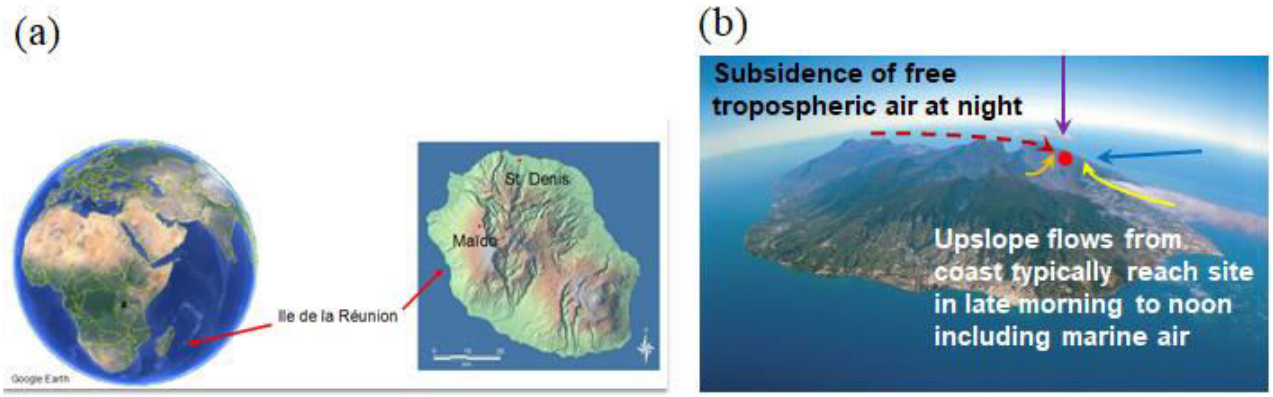

Figure 2.1 (a) Location of the high-altitude Maïdo observatory on the remote island of La Réunion in the southwest IO, and (b) a map of the island where the solid red circle indicates the position of the observatory with typical air flow in the daytime and nighttime the sampling period (March 15-April 24, 2018).

Previous studies reported that the observatory is located in the MBL during the daytime, and in the FT during nighttime (Baray et al., 2013; Guilpart et al., 2017) (**Figure 2.2**). Although Collaud Coen et al. (2018) pointed to the influence of residual aerosols in the daytime on nighttime conditions at high-altitude stations, Guilpart et al. (2017) showed a one-year long record of the isotopic composition of water vapor at the same observatory to demonstrate the validity of the assumption of FT conditions at night. Thus, aerosol samples were obtained in the daytime and nighttime conditions using two identical aerosol samplers, as described in the following subsection.

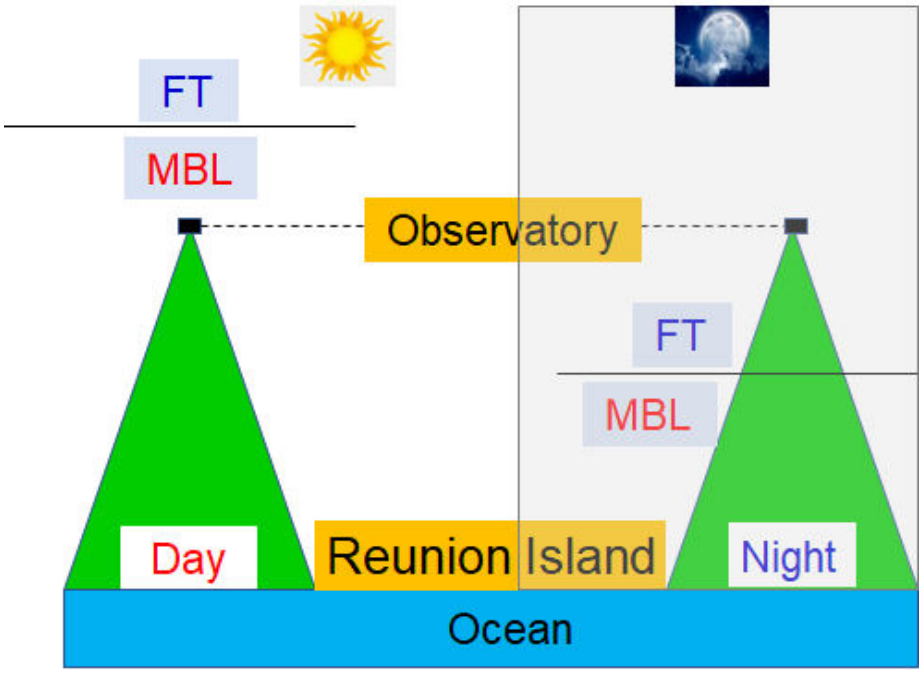

Figure 2.2 Conceptual scheme of the high-altitude Maïdo observatory in the daytime and the nighttime, which correspond to conditions of the marine boundary layer (MBL) and free troposphere (FT), respectively.

2.2 Aerosol sampling

Submicrometer aerosol samples were collected at the Maïdo observatory during the period of March 15–May 24, 2018, in the framework of the OCTAVE (Oxygenated Compounds in the Tropical Atmosphere: Variability and Exchanges) project (e.g., Verreyken et al., 2020). The objectives of the project are to improve the global budget of key VOCs and their role in tropical regions, relying on an integrated approach combining in situ measurements, satellite retrievals, and modeling. Participating organizations in the project are: Royal Belgian Institute for Space Aeronomy (BIRA-IASB), Université Libre de Bruxelles (ULB), Université de La Réunion,

Réunion (CNRS-LACy), Laboratoire de météorologie physique (LAMP), Univ. of Colorado Boulder, and Hokkaido University.

The aerosol samplings were conducted continuously using two high-volume air samplers (HVAS; Model 120SL, Kimoto Electric, Osaka, Japan) in parallel (**Figure 2.3**), with cascade impactors (Model-TE 234, Tisch Environmental, Inc., Cleves, OH, USA) attached to each. The samples were collected onto quartz-fiber filters at a flow rate of 1130 L min^{-1} with one sampler during daytime (0700–1800 in local time; LT) and the other sampler during nighttime (2200–0500 LT) by the auto power supply. To avoid the influence of the residual layer on the separation between MBL and FT conditions, 1800–2200 LT and 0500–0700 LT were set to be a transition time. After the sample collection, the filter samples were stored in the glass vial with a Teflon-lined screw cap at −20ºC in a freezer prior to the analysis.

Figure 2.3 Two high-volume air samplers (HVAS; Model 120SL, Kimoto Electric, Osaka, Japan) in parallel located at the observatory (left). One sampler was used for the daytime sampling, and the other was used for the nighttime sampling. The power was supplied for each sampler automatically using a timer (right).

In this study, analytical results obtained from the bottom stage of the impactor, which collected particles with aerodynamic diameters (D_p) lower than 0.95 μm were used. Here, ambient aerosol particles collected at the bottom are referred to as submicrometer aerosol particles. The sample filters were typically exchanged every two to three days. The average volumes of the sampled air were 2098 m^3 and 1454 m^3 during daytime and nighttime, respectively.

2.3 Measurements of chemical parameters of water-soluble aerosols

2.3.1 Water-soluble organic carbon (WSOC)

In this study, the term "water-soluble aerosols" is defined as particles sampled on the filter and extracted with ultrapure water followed by filtration through a 0.22-μm syringe filter (Miyazaki et al., 2018). To determine concentrations of water-soluble organic carbon (WSOC) in the submicrometer filter samples, a filter cut of 39.25 cm^2 was extracted with 15 mL ultrapure water using an ultrasonic bath for 15 min. The ultrapure water was generated by a Sartorius Stedim Biotech arium pro ultrapure water system (Model 611: Sartorius AG, Goettingen, Germany). The extracts were then filtrated with a disc filter (Millex-GV, 0.22 μm, Millipore, Billerica, MA, USA), followed by the injection of the dissolved organic carbon in the extracts into a total organic carbon analyzer (Model TOC-Lchp, Shimadzu, Kyoto, Japan) (Miyazaki et al., 2018, 2020). The WSOC mass of a field blank corresponded to less than ~20 % of that in the ambient samples. All the data of the WSOC concentration presented here were corrected against field blanks.

2.3.2 Stable carbon isotope ratios of WSOC

To measure the stable carbon isotope ratios of WSOC ($\delta^{13}C_{WSOC}$, ‰ relative to VPDB), another filter cut (27.24 cm^2) for each sample was acidified to pH 2 with hydrochloric acid (HCl) to remove inorganic carbon prior to extraction (Miyazaki et al., 2018, 2020). The decarbonated filter samples were then dried under a nitrogen stream for approximately 2 h. WSOC was extracted from the filters in 20 mL of ultrapure water using the same method described above. The extracted samples were concentrated by rotary evaporation, and 40 μL of each sample was transferred to 10 mg of pre-combusted Chromosorb absorbent in a pre-cleaned tin cup. The $\delta^{13}C_{WSOC}$ values were then measured with a Flash EA 1112 continuous flow carrier gas system (ConFlo) - Delta V isotope

ratio mass spectrometer (Thermo Fisher Scientific). The $\delta^{13}C$data are reported relative to an established reference of carbon Vienna Pee Dee Belemnite (VPDB).

2.3.3 Inorganic species

To determine the concentrations of inorganic ions, another filter cut (19.63 cm^2) was extracted with ultrapure water. The total extract was filtered through a membrane disc filter, and major inorganic ions (SO_4^{2-}, NO_3^-, NO_2^-, Cl^-, Br^-, NH_4^+, Na^+, K^+, Ca^{2+}, and Mg^{2+}), including methanesulfonic acid (MSA), were determined with an ion chromatograph (Model 761 compact IC; Metrohm, Herisau, Switzerland) (Miyazaki et al., 2016). Field blanks of MSA corresponded to less than ~9% of the average concentrations of the ambient samples, whereas the blank values of the other inorganic ions were less than 1% of the ambient concentrations.

2.3.4 Aerosol organic carbon (OC)

The amounts of organic carbon (OC) on the filter punches (1.54 cm^2) were determined using a sunset lab carbon analyzer following the Interagency Monitoring of Protected Visual Environments (IMPROVE) thermal evolution protocol. Aerosol samples were collected, and then the concentrations of OC were analyzed by a thermal optical transmittance (TOT) method. The samples were heated sequentially in four steps, 300°C, 450°C, 600°C, and 740°C, in a completely oxygen-free atmosphere for the OC analysis. All the carbon components of carbonaceous aerosols were converted to CO_2 and were detected with a nondispersive infrared absorption (NDIR) sensor. OC was automatically quantified by dividing their peak areas by the internal calibration peak made by methane gas (5% CH_4 in He) (Miyazaki et al., 2016).

2.4 Measurements of molecular tracer compounds

Another portion of the filter (58.9 cm^2) was extracted with dichloromethane/methanol to measure biogenic molecular tracers. Filter aliquots were extracted three times with dichloromethane/methanol (2:1; v/v) under ultrasonication for 10 min every time. The solvent extracts were filtered through quartz wool packed in a Pasteur pipette, concentrated by using a rotary evaporator under vacuum, and blown down to dryness with pure nitrogen gas. The extracts were then reacted with 60 μL of N,O-bis-(trimethylsilyl)trifluoroacetamide (BSTFA) at 70°C for 3 h to convert –COOH to TMS esters and –OH to TMS ethers (Fu et al., 2011). After the reaction, the derivatives were diluted with the internal standard (140 μL) and then analyzed for the compounds listed above using a capillary gas chromatograph (GC8890, Agilent) coupled to a mass spectrometer (MSD5977B, Agilent).The measured molecular compounds include 2-methyltetrol, pinic acid, pinonic acid, and 3-methyl-1,2,3-butanetricarboxylic acid (3-MBTCA), as oxidation products of biogenic VOCs (Yu et al., 1999; Claeys et al., 2004; 2007; Szmigielski et al., 2007). In addition, tracers of primary biogenic emissions, such as glucose (Simoneit et al., 2004) and *n*-nonacosan-10-ol (Miyazaki et al., 2019), were also measured.

2.5 Meteorological parameters and FLEXPART backward trajectory

Meteorological parameters (for example: temperature, relative humidity, rain quantity, wind speed, etc.) were recorded every 3 minutes by meteorological sensors (Vaisala, Helsinki, Finland) at the Maïdo observatory for the sampling period. Then the average values of meteorological parameters were merged into the duration of aerosol sampling for both day and nighttime separately. Water vapor mixing ratio values at the sampling site were derived to confirm seasonal

and diurnal changes from the measured ambient temperature and relative humidity. An equation for calculating water vapor mixing ratios is given below:

$$\text{Water vapor mixing ratio} = 0.622 \times e/P \ (g\ kg^{-1})$$

where e and P refer to water vapor pressure and air pressure, respectively.

To investigate air mass histories from the sampling site, ten-day backward trajectories were computed using the Lagrangian FLEXible PARTicle dispersion model, FLEXPART (Stohl et al., 1998; Pisso et al., 2019). These FLEXPART simulations were driven with hourly European Centre for Medium-Range Weather Forecasts (ECMWF) operational data at half a degree horizontal resolution and 137 vertical levels. The calculation was initialized at 00, 06, 12, and 18 UTC every day during the sampling period.

2.6 Positive Matrix Factorization

Positive Matrix Factorization (PMF) (Paatero and Tapper, 1994) is used to identify and characterize possible sources of the observed WSOC during the study period. PMF model reduces large number of variables in complex analytical data sets to combinations of species called source types and source contributions. The source types are identified by comparing them to measured profiles. Source contributions are used to determine how much each source contributed to a sample. The model calculates source profiles or fingerprints, source contributions, and source profile uncertainties. The PMF model results are constrained to provide positive source

contributions and the uncertainty weighted difference between the observed and predicted species concentration is minimized.

In this study, EPA PMF 5.0 (Norris et al., 2014) was used for the calculation with inputs of mass concentrations of sixteen chemical components (WSOC, glucose, *n*-nonacosan-10-ol, 2-methyltetrol, pinic acid, pinonic acid, 3-MBTCA, SO_4^{2-}, NO_3^-, NH_4^+, Na^+, MSA, Br^-, K^+, Ca^{2+}, and Mg^{2+}). The analytical measurement uncertainties of each component were derived in each analysis and were used as uncertainties in the PMF model. The calculation was performed with 20 runs. PMF outputs were explored by varying the number of factors systematically, to check Q values (i.e., values reached by the objective function which is minimized by the PMF model), distribution of residuals, physical sense of source profiles and contributions (**Table 2.1**). As a result, 6 factors were the most appropriate number of factors corresponding to meaningful sources. The PMF reproduced more than 86% of the measured mass concentrations of WSOC.

Table 2.1 Numbers of factors obtained for PMF solutions along with Q-values (i.e., values reached by the objective function which is minimized by the model), scaled residuals, and squared correlation coefficients (r^2) for WSOC. Based on Q values, distributions of scaled residuals, and r^2, as well as a physical sense of source profiles and contributions, 6 factors were the most appropriate number of factors corresponding to meaningful sources in this study.

Total number of factors	Q (Robust)	Q (True)	Q (True) / Q (Robust)	Scaled residuals beyond 3 standard deviations for WSOC	r^2 for WSOC
4	36826	2766324	75.1	−4.75, −3.83, −3.28, 3.02, 3.29, 3.55, 3.80,4.18, 4.47, 4.65, 6.43, 7.66, 7.95	0.58
5	27261	2033453	74.6	−3.48, −3.28, 3.27, 3.45, 3.73, 4.45, 6.54	0.78
6	18171	766656	42.2	3.15, 3.44, 3.90	0.86
7	10113	107990	10.7	−3.35, −3.13, 3.13, 3.59	0.86

References

Baray, J. L., Courcoux, Y., Keckhut, P., Portafaix, T., Tulet, P., Cammas, J. P., Hauchecorne, A., Godin Beekmann, S., De Mazière, M., Hermans, C., Desmet, F., Sellegri, K., Colomb, A., Ramonet, M., Sciare, J., Vuillemin, C., Hoareau, C., Dionisi, D., Duflot, V., Vérèmes, H., Porteneuve, J., Gabarrot, F., Gaudo, T., Metzger, J. M., Payen, G., Leclair De Bellevue, J., Barthe, C., Posny, F., Ricaud, P., Abchiche, A. and Delmas, R.: Maïdo observatory: A new high-altitude station facility at Reunion Island (21 S, 55 E) for long-term atmospheric remote sensing and in situ measurements, Atmos. Meas. Tech., 6, 2865–2877, https://doi.org/10.5194/amt-6-2865-2013, 2013.

Claeys, M., Graham, B., Vas, G., Wang, W., Vermeylen, R., Pashynska, V., Cafmeyer, J., Guyon, P., Andreae, M. O., Artaxo, P. and Maenhaut, W.: Formation of secondary organic aerosols through photooxidation of Isoprene, Science, 303, 1173–1176, https://doi.org/10.1126/science.1092805, 2004.

Claeys, M., Szmigielski, R., Kourtchev, I., Van Der Veken, P., Vermeylen, R., Maenhaut, W., Jaoui, M., Kleindienst, T. E., Lewandowski, M., Offenberg, J. H. and Edney, E. O.: Hydroxydicarboxylic acids: Markers for secondary organic aerosol from the photooxidation of α-pinene, Environ. Sci. Technol., 41, 1628–1634, https://doi.org/10.1021/es0620181, 2007.

Collaud Coen, M., Andrews, E., Aliaga, D., Andrade, M., Angelov, H., Bukowiecki, N., Ealo, M., Fialho, P., Flentje, H., Hallar, A. G., Hooda, R., Kalapov, I., Krejci, R., Lin, N.-H., Marinoni, A., Ming, J., Nguyen, N. A., Pandolfi, M., Pont, V., Ries, L., Rodríguez, S., Schauer, G., Sellegri, K., Sharma, S., Sun, J., Tunved, P., Velasquez, P., and Ruffieux, D.: Identification of topographic features influencing aerosol observations at high altitude stations, Atmos.

Chem. Phys., 18, 12289–12313, https://doi.org/10.5194/acp-18-12289-2018, 2018.

Fu, P., Kawamura, K. and Miura, K.: Molecular characterization of marine organic aerosols collected during a round-the-world cruise, J. Geophys. Res.-Atmos., 116, D13302, https://doi.org/10.1029/2011JD015604, 2011.

Guilpart, E., Vimeux, F., Evan, S., Brioude, J., Metzger, J. M., Barthe, C., Risi, C. and Cattani, O.: The isotopic composition of near-surface water vapor at the Maïdo observatory (Reunion Island, southwestern Indian Ocean) documents the controls of the humidity of the subtropical troposphere, J. Geophys. Res.-Atmos., 122, 9628–9650, https://doi:10.1002/2017JD026791, 2017.

Miyazaki, Y., Coburn, S., Ono, K., Ho, D. T., Pierce, R. B., Kawamura, K. and Volkamer, R.: Contribution of dissolved organic matter to submicron water-soluble organic aerosols in the marine boundary layer over the eastern equatorial Pacific, Atmos. Chem. Phys., 16, 7695–7707, https://doi.org/10.5194/acp-16-7695-2016, 2016.

Miyazaki, Y., Yamashita, Y., Kawana, K., Tachibana, E., Kagami, S., Mochida, M., Suzuki, K. and Nishioka, J.: Chemical transfer of dissolved organic matter from surface seawater to sea spray water-soluble organic aerosol in the marine atmosphere, Sci. Rep., 8, 1–10, https://doi.org/10.1038/s41598-018-32864-7, 2018.

Miyazaki, Y., Gowda, D., Tachibana, E., Takahashi, Y. and Hiura, T.: Identification of secondary fatty alcohols in atmospheric aerosols in temperate forests, Biogeosciences, 16, 2181–2188, https://doi.org/10.5194/bg-16-2181-2019, 2019.

Miyazaki, Y., Suzuki, K., Tachibana, E., Yamashita, Y., Müller, A., Kawana, K. and Nishioka, J.: New index of organic mass enrichment in sea spray aerosols linked with senescent status in marine phytoplankton, Sci. Rep., 10, 1–10, https://doi.org/10.1038/s41598-020-73718-5,

2020.

Norris, G., Duvall, R., Brown, S. and Bai, S.: EPA Positive Matrix Factorization (PMF) 5.0 Fundamentals and User Guide. Washington, DC: Environmental Protection Agency, Office of Research and Development, Available at: https://www.epa.gov (last access: 13 July 2021), 2014.

Paatero, P. and Tapper, U.: Positive matrix factorization: a nonnegative factor model with optimal utilization of error estimates of data values, Environmetrics, 5, 111 – 126, 1994.

Pisso, I., Sollum, E., Grythe, H., Kristiansen, N. I., Cassiani, M., Eckhardt, S., Arnold, D., Morton, D., Thompson, R. L., Groot Zwaaftink, C. D., Evangeliou, N., Sodemann, H., Haimberger, L., Henne, S., Brunner, D., Burkhart, J. F., Fouilloux, A., Brioude, J., Philipp, A., Seibert, P. and Stohl, A.: The Lagrangian particle dispersion model FLEXPART version 10.4, Geosci. Model Dev., 12, 4955–4997, https://doi.org/10.5194/gmd-12-4955-2019, 2019.

Simoneit, B. R. T., Elias, V. O., Kobayashi, M., Kawamura, K., Rushdi, A. I., Medeiros, P. M., Rogge, W. F. and Didyk, B. M.: Sugars - Dominant water-soluble organic compounds in soils and characterization as tracers in atmospheric participate matter, Environ. Sci. Technol., 38, 5939–5949, https://doi.org/10.1021/es0403099, 2004.

Stohl, A., Hittenberger, M. and Wotawa, G.: Validation of the Lagrangian particle dispersion model FLEXPART against large-scale tracer experiment data, Atmos. Environ., 32, 4245–4264, https://doi.org/10.1016/S1352-2310(98)00184-8, 1998.

Szmigielski, R., Surratt, J. D., Gómez-González, Y., van der Veken, P., Kourtchev, I., Vermeylen, R., Blockhuys, F., Jaoui, M., Kleindienst, T. E., Lewandowski, M., Offenberg, J. H., Edney, E. O., Seinfeld, J. H., Maenhaut, W. and Claeys, M.: 3-methyl-1,2,3-butanetricarboxylic acid: An atmospheric tracer for terpene secondary organic aerosol, Geophys. Res. Lett., 34,

L24811, https://doi.org/10.1029/2007GL031338, 2007.

Verreyken, B., Amelynck, C., Brioude, J., Muller, J. F., Schoon, N., Kumps, N., Colomb, A., Metzger, J. M., Lee, C. F., Koenig, T. K., Volkamer, R. and Stavrakou, T.: Characterisation of African biomass burning plumes and impacts on the atmospheric composition over the south-west Indian Ocean, Atmos. Chem. Phys., 20, 14821–14845, https://doi.org/10.5194/acp-20-14821-2020, 2020.

Yu, J., Cocker III, D. R., Griffin, R. J., Flagan, R. C. and Seinfeld, J. H.: Journal of Atmospheric Chemistry, Volume 34, Number 2 - SpringerLink, J. Atmos. Chem., 34, 207–258, 1999.

Chapter 3. Characterization of Meteorological Parameters, Marine Primary Productivity, and Aerosol Organic Carbon (OC) in the Tropical Indian Ocean

3.1 Introduction

The biogeochemical linkage between the ocean surface and the atmosphere is a major factor controlling the effect of the ocean on climate and the feedback to the ocean biology (Morel and Price, 2003; York, 2018). The Indian Ocean (IO) plays an important role in regulating not only regional meteorology but also global climate change (Hermes et al., 2019; Roxy et al., 2020). The western IO has one of the largest phytoplankton blooms among the tropical oceans, particularly in summer (Koné et al., 2009; Roxy et al., 2016). Elevated primary productivity is supported by a large amount of nutrients supplied by a strong coastal and open ocean upwelling over this oceanic region (Koné et al., 2009; Lévy et al., 2007). Relatively high marine primary productivity is expected to produce a significant amount of organic carbon (OC), followed by being emitted into the atmosphere to subsequently affect the physicochemical properties of aerosols and clouds. However, there have been few studies on linkages among meteorological parameters, marine primary productivity, and atmospheric aerosol OC in this oceanic region. In this chapter, the meteorological parameters, marine primary productivity, and their linkage with aerosol OC will be discussed.

3.2 Water vapor mixing ratio as diagnostics of wet vs. dry seasons and marine boundary layer vs. free tropospheric conditions

To define seasonal categories and to verify diurnal changes in the atmospheric conditions around the sampling site, the water vapor mixing ratio was calculated by the method described in Chapter 2. **Figure 3.1** shows the time series of the water vapor mixing ratios in daytime and nighttime during the entire sampling period. It is apparent that the water vapor mixing ratios substantially decreased just after April 24, both in the daytime and nighttime. The average mixing ratios of water vapor were 8.7 ± 2.6 g kg^{-1} and 6.4 ± 1.4 g kg^{-1} during the first half (March 15–April 23, 2018) and the second half (April 24–May 24, 2018) of the sampling period, respectively. In this study, the first half of the sampling period was defined as the wet season, whereas the latter half was defined as the dry season.

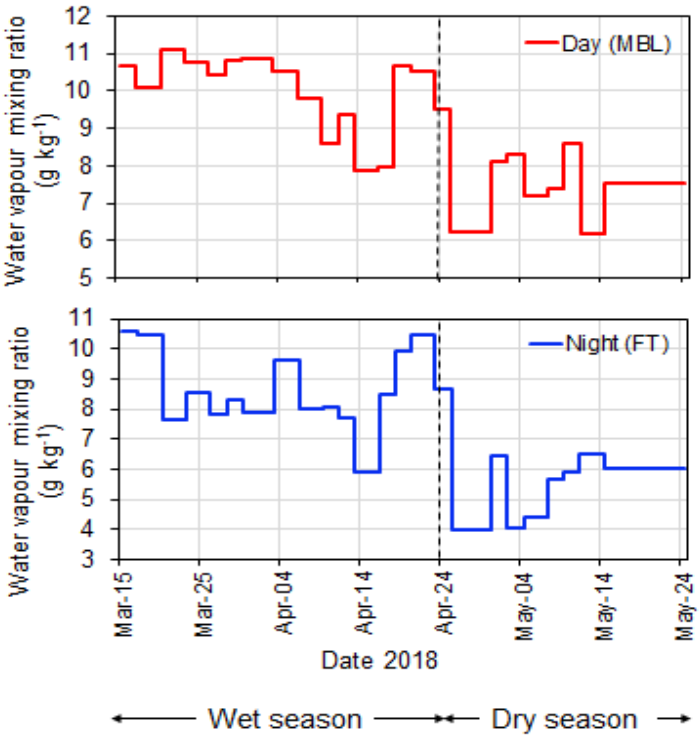

Figure 3.1 Time series of the water vapor mixing ratios in the daytime (MBL) and nighttime (FT).

Water vapor mixing ratios during daytime (9.3 ± 2.7 g kg^{-1} and 8.1 ± 2.5 g kg^{-1} for wet and dry seasons, respectively) were significantly higher than those observed during nighttime (7.4 ± 0.9 g kg^{-1} and 5.4 ± 1.4 g kg^{-1} for the wet and dry seasons, respectively) (**Figure 3.2**). Guilpart et al. (2017) presented a one-year record of the mixing ratio of water vapor at the Maïdo observatory, demonstrating a clear seasonal decrease in the mixing ratio from March to May. Moreover, they reported distinct diurnal variations in the water vapor mixing ratio with averages of 9.7 ± 2.4 g kg^{-1} during the day (0700–1800 LT) and 6.4 ± 2.9 g kg^{-1} at night (2200–0500 LT) during the one-year period, showing that the Maïdo observatory indeed located both in the MBL and FT during the day and at night, respectively. The observed levels of the water vapor mixing ratio and their seasonal changes in this study are consistent with those reported by Guilpart et al. (2017). Therefore, the results presented confirm that the observatory was located in the MBL during the daytime, whereas it was in the FT at night.

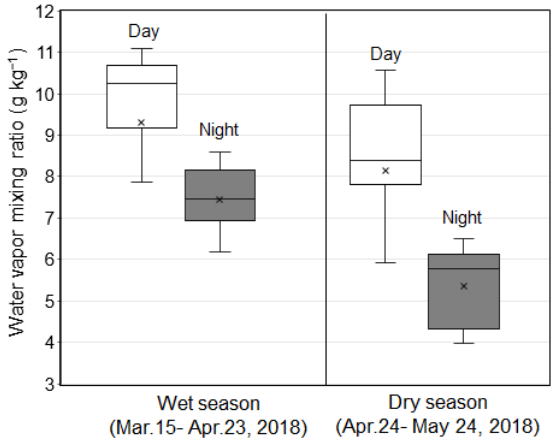

Figure 3.2 Box-whisker plots of the water vapor mixing ratio during the first half (Mar 15–Apr 23, 2018) and the second half (Apr 24–May 24, 2018) of the sampling period. White and gray box plots indicate the data for daytime (0700–1800 LT) and nighttime (2200–0500 LT), respectively; medians and the upper/lower 25 percentile of data are shown. Cross marks indicate the average values of each category.

3.3 Meteorological parameters, marine primary productivity, and their link with aerosol organic carbon (OC)

Table 3.1 summarizes the average temperature, relative humidity, rain quantity, and atmospheric pressure at the observatory under the MBL (day) and FT (night) conditions during the wet and dry seasons. The average temperature during the wet season (14.1 ± 0.6ºC and 12.1 ± 1.3ºC in MBL and FT, respectively) was slightly higher than that during the dry season (13.0 ± 1.1ºC and 10.6 ± 1.2ºC in MBL and FT, respectively). On the other hand, relative humidity in the wet season (80 ± 8% and 78 ± 8% in MBL and FT, respectively) was significantly higher than that in the dry season (64 ± 11% and 54 ± 12% in MBL and FT, respectively). Similarly, rain quantity was significantly higher during the wet season (7.5 ± 18 l m^{-2} and 6.2 ± 11 l m^{-2} in MBL and FT, respectively) than in the dry season when no rain was observed. The values of the meteorological parameters justify the definition of wet and dry seasons in this study.

Table 3.1. Average concentrations and standard deviations of the meteorological parameters under the marine boundary layer (MBL; daytime) and free tropospheric (FT; nighttime) conditions at the Maïdo observatory during wet and dry seasons.

	Wet season (Mar 15–Apr 23, 2018)		Dry season (Apr 24–May 24, 2018)	
	MBL (day) *n* = 16	FT (night) *n* = 16	MBL (day) *n* = 8	FT (night) *n* = 8
Temperature (ºC)	14.1 ± 0.6	12.1 ± 1.3	13.0 ± 1.1	10.6 ± 1.2
Relative humidity (%)	80 ± 8	78 ± 8	64 ± 11	54 ± 12
Rain quantity (l m^{-2})	7.5 ± 18	6.2 ± 11	0 ± 0	0 ± 0
Air pressure (hPa)	789 ± 1.4	788 ± 1.3	791 ± 0.9	790 ± 0.8

Figure 3.3 shows the time series of air pressure measured at the sampling site under the MBL and FT conditions during the entire aerosol sampling period. It is apparent that the air pressure during the wet season (789 ± 1.4 hPa and 788 ± 1.3 hPa in MBL and FT, respectively) was generally lower than that in the dry season (791 ± 0.9 hPa and 790 ± 0.8 hPa in MBL and FT, respectively). The lower air pressure in the wet season is generally linked with more active vertical transport of air from the ocean surface. In addition, the air pressure showed variations on a timescale of approximately a week to 10 days during the wet season. This reflects the synoptic-scale meteorology around the sampling location.

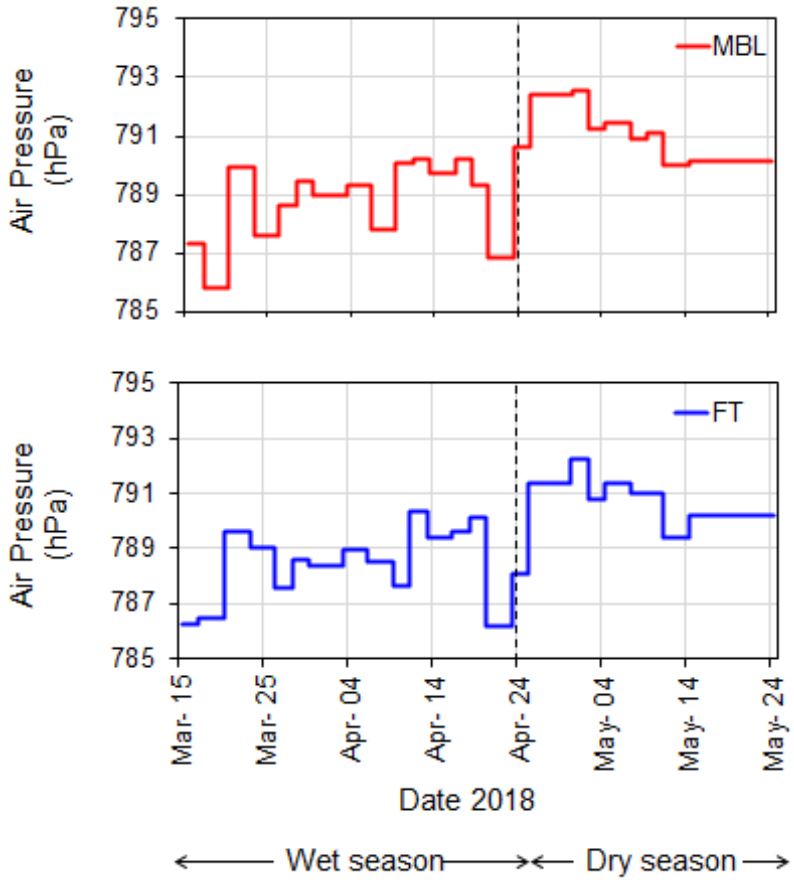

Figure 3.3 Time series of the air pressure at the sampling site under the MBL (in the daytime) and FT (in the nighttime) conditions throughout the sampling period.

Figure 3.4 shows the marine primary productivity over IO during the study period, which was classified into three months. The marine primary productivity over IO was largest in March (wet season), which tended to decrease from March to May (dry season). The high marine primary productivity in the wet season was induced by light, nutrients, micronutrients, CO_2, and temperature together with transport of seawater in the ocean including upwelling (Boyd et.al., 2014).

As described in section 3.1, the large phytoplankton blooms were evident in coastal and pelagic regions of the western IO in March. The overall results, including the meteorological parameters, suggest that the wet season is characterized by higher marine primary productivity and atmospheric relative humidity than in dry season with more evident synoptic-scale meteorology, which accompanies more active vertical transport of air from the ocean surface.

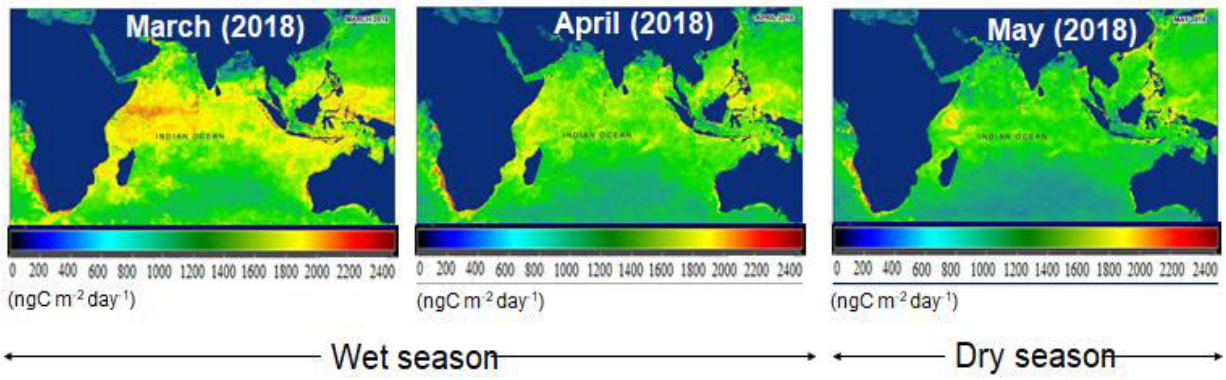

Figure 3.4 Marine primary productivity over the Indian Ocean in March, April, and May 2018. The colors in the map explain the productivity condition of the ocean. Blue (0–1200 ngC $m^{-2}day^{-1}$), green (1200–1800 ngC $m^{-2}day^{-1}$) and from yellow to red (1800–2400 ngC $m^{-2}day^{-1}$) colors indicate oligotrophic, mesotrophic, and eutrophic states of the oceanic regions, respectively (Carr et al., 2006; Istvánovics, 2009). The figure was produced and adapted from the Ocean Productivity web (http://sites.science.oregonstate.edu/ocean.productivity/index.php). Net Primary Production was derived using the Eppley-VGPM (Vertically Generalized Production Model) algorithm.

To investigate a linkage between the meteorological parameters and the atmospheric aerosol concentrations of organic matter, **Figure 3.5** shows the times series of the mass concentrations of organic carbon (OC) and water-soluble OC (WSOC) in MBL and FT during the entire sampling period. In MBL, the OC concentrations during the wet season were generally larger than those during the dry season. The larger concentrations of OC during the wet season likely reflect higher marine primary productivity and more active vertical transport of air from the ocean surface as described above. The vertical transport of the aerosol particles over the open ocean was mainly caused by convection (Babu and Sivaprasad, 2014). The temporal trend of WSOC is similar to that of OC for both MBL and FT conditions particularly during the wet season, when the average WSOC/OC ratios were 46 ± 16% and 26 ± 13% in MBL and FT, respectively. The result indicates that the water-soluble fraction of OC was an important factor controlling the total organic matter in the submicrometer aerosols during the wet season in this study. The specific source and formation processes of WSOC are discussed in Chapter 4.

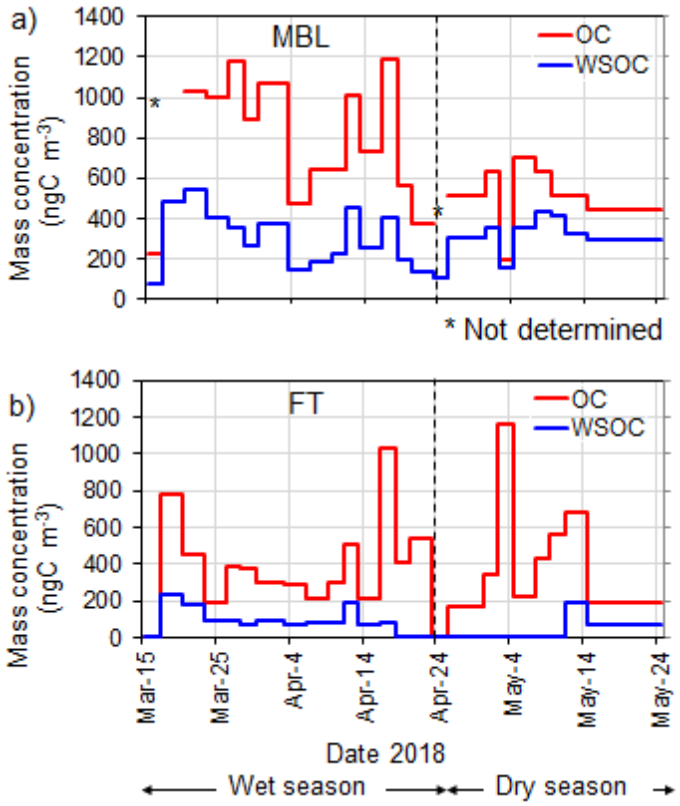

Figure 3.5 Time series of organic carbon (OC) and water-soluble OC (WSOC) concentrations under the (a) MBL (daytime) and (b) FT (nighttime) conditions during the entire sampling period.

3.4 Conclusions

The observed levels of the water vapor mixing ratio and their seasonal changes at the high-altitude Maïdo observatory confirm that the observatory was located in the MBL during the daytime, whereas it was in the FT at night. This is also supported by previous studies. The seasonal changes in the meteorological parameters and marine primary productivity suggest that the wet season is characterized by higher marine primary productivity and atmospheric relative humidity than in the dry season. In addition, synoptic-scale meteorology is more evident which accompanies more active vertical transport of air from the ocean surface. In MBL, the OC concentrations during the wet season were generally higher than those during the dry season, which likely reflect higher

marine primary productivity and more active vertical transport of air from the ocean surface. The temporal trends of OC and WSOC suggest that the water-soluble fraction of OC was an important factor controlling the total organic matter in the submicrometer aerosols during the wet season.

References

Babu, C. A. and Sivaprasad, P.: Variability and mechanisms of vertical distribution of aerosols over the Indian region, Int. J. Remote Sens., 35, 7691–7705, doi:10.1080/01431161.2014.975379, 2014.

Black, E., Slingo, J. M. & Sperber, K. R.: An observational study of the relationship between excessively strong short rains in coastal East Africa and Indian Ocean SST, Mon. Weather Rev., 131, 74–94, https://doi.org/10.1175/1520-0493, 2003.

Boyd, P.W., Sundby, S. and Pörtner, H.O.: Cross-chapter box on net primary production in the ocean, In: Climate Change 2014: Impacts, Adaptation, and Vulnerability, Part A: Global and Sectoral Aspects, Contribution of Working Group II to the Fifth Assessment Report of the Intergovernmental Panel on Climate Change, Cambridge University Press, Cambridge, United Kingdom and New York, NY, USA, 133-136, available at: https://epic.awi.de/id/eprint/37516/1/CC_PrimaryProduction.pdf, 2014.

Carr, M. E., Friedrichs, M. A. M., Schmeltz, M., Noguchi Aita, M., Antoine, D., Arrigo, K. R., Asanuma, I., Aumont, O., Barber, R., Behrenfeld, M., Bidigare, R., Buitenhuis, E. T., Campbell, J., Ciotti, A., Dierssen, H., Dowell, M., Dunne, J., Esaias, W., Gentili, B., Gregg, W., Groom, S., Hoepffner, N., Ishizaka, J., Kameda, T., Le Quéré, C., Lohrenz, S., Marra, J., Mélin, F., Moore, K., Morel, A., Reddy, T. E., Ryan, J., Scardi, M., Smyth, T., Turpie, K., Tilstone, G., Waters, K. and Yamanaka, Y.: A comparison of global estimates of marine primary production from ocean color, Deep-Sea Res. Pt. II, 53, 741–770, https://doi.org/10.1016/j.dsr2.2006.01.028, 2006.

Goddard, L. & Graham, N. E.: Importance of the Indian Ocean for simulating rainfall anomalies over eastern and southern Africa, J. Geophys. Res., 104, 19,099–19,116, http://doi.org/10.1029/1999JD900326, 1999.

Guilpart, E., Vimeux, F., Evan, S., Brioude, J., Metzger, J. M., Barthe, C., Risi, C. and Cattani, O.: The isotopic composition of near-surface water vapor at the Maïdo observatory (Reunion Island, southwestern Indian Ocean) documents the controls of the humidity of the subtropical troposphere, J. Geophys. Res.-Atmos., 122, 9628–9650, https://doi.org/10.1002/2017JD026791, 2017.

Hermes, J. C., Masumoto, Y., Beal, L. M., Roxy, M. K., Vialard, J., Andres, M., Annamalai, H., Behera, S., D'Adamo, N., Doi, T., Feng, M., Han, W., Hardman-Mountford, N., Hendon, H., Hood, R., Kido, S., Lee, C., Lee, T., Lengaigne, M., Li, J., Lumpkin, R., Navaneeth, K. N., Milligan, B., McPhaden, M. J., Ravichandran, M., Shinoda, T., Singh, A., Sloyan, B., Strutton, P. G., Subramanian, A. C., Thurston, S., Tozuka, T., Ummenhofer, C. C., Unnikrishnan, A. S., Venkatesan, R., Wang, D., Wiggert, J., Yu, L. and Yu, W.: A sustained ocean observing system in the indian ocean for climate related scientific knowledge and societal needs, Front. Mar. Sci., 6, 1–21, https://doi.org/10.3389/fmars.2019.00355, 2019.

Istvánovics, V.: Eutrophication of Lakes and Reservoirs, Encycl. Inl. Waters, 157–165, https://doi.org/10.1016/B978-012370626-3.00141-1, 2009.

Koné, V., Aumont, O., Lévy, M. and Resplandy, L.: Physical and biogeochemical controls of the phytoplankton seasonal cycle in the Indian Ocean: A modeling study, Geophys. Monogr. Ser., 185, 147–166, https://doi:10.1029/2008GM000700, 2009.

Krishnan R., Sanjay J., Gnanaseelan C., Mujumdar M., Kulkarni A. and Chakraborty S.: Assessment of Climate Change over the Indian Region, chapter: Indian Ocean Warming, Springer, 191-206, https://doi.org/10.1007/978-981-15-4327-2_10, 2020.

Lévy, M., Shankar D., J. André M., Shenoi S., Durand F. and Montegut C. B.: Basin-wide seasonal evolution of the Indian Ocean's phytoplankton blooms, J. Geophys. Res., 112, C12014, https://doi:10.1029/2007JC004090, 2007.

Morel, F. M. M. and Price, N. M.: The biogeochemical cycles of trace metals in the oceans, Science, 300, 944–947, https://doi.org/10.1126/science.1083545, 2003.

Roxy, M. K., Modi, A., Murtugudde, R., Valsala, V., Panickal, S., Prasanna Kumar, S., Ravichandran, M., Vichi, M. and Lévy, M.: A reduction in marine primary productivity driven by rapid warming over the tropical Indian Ocean, Geophys. Res. Lett., 43, 826–833, https://doi:10.1002/2015GL066979, 2016.

Slingo, J., Spencer, H., Hoskins, B., Berrisford, P. and Black, E.: The meteorology of the Western Indian Ocean, and the influence of the East African Highlands, Philos. Trans. R. Soc. A Math. Phys. Eng. Sci., 363, 25–42, https://doi:10.1098/rsta.2004.1473, 2005.

York, A.: Environmental microbiology: Marine biogeochemical cycles in a changing world, Nat. Rev. Microbiol., 16, 259, https://doi:10.1038/nrmicro.2018.40, 2018.

Chapter 4. Origin of Water-Soluble Organic Aerosols at the Maïdo High-altitude Observatory, Réunion Island in the Tropical Indian Ocean

4.1 Introduction

It has been expected that the tropical and subtropical Indian Ocean (IO) is a major source of water-soluble organic aerosols (WSOAs), which are important factors relevant to the cloud formation of aerosol particles. Current atmospheric numerical models significantly underestimate the budget of organic aerosols and their precursors, especially over tropical oceans. This is primarily due to poor knowledge of sources and paucity of observations on spatial and temporal variations of aerosol chemical parameters over the tropical open ocean. To evaluate the contribution of each source to WSOA as well as their formation processes, submicrometer aerosol sampling was conducted at the high-altitude Maïdo observatory (21.1° S, 55.4° E, 2,160 m a.s.l), located on the remote island of La Réunion in the southwest IO. In this chapter, the origin and formation process of WSOC in the study area will be discussed.

4.2 Seasonal variations of mass fractions and concentrations of submicrometer water-soluble aerosol

Figure 4.1 shows seasonal changes in chemical mass fraction of the submicrometer water-soluble aerosols under the MBL and FT conditions during the entire sampling period. Water-soluble organic matter (WSOM) dominated the aerosol mass in the MBL (46 ± 10%) and in the FT (43 ± 23%) during the wet season. In contrast, during the dry season, sulfate was the dominant component of the submicrometer water-soluble aerosol mass in both the MBL (77 ± 19%) and in the FT (76 ± 15%). The pattern of the temporal variation of the mass fractions was similar in MBL and FT in both seasons.

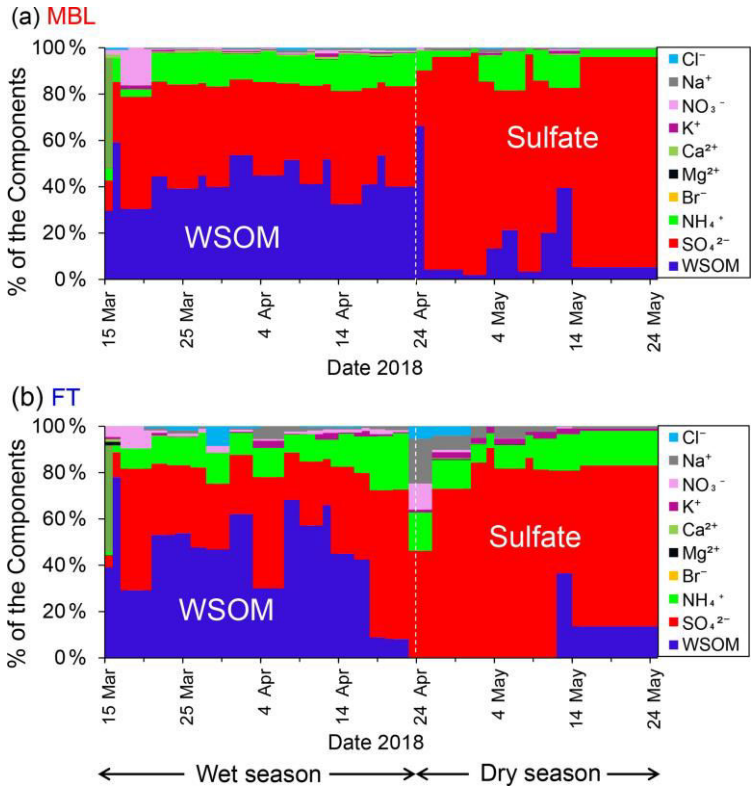

Figure 4.1 Time series of the chemical mass fraction of the submicrometer water-soluble aerosols under (a) MBL (in the daytime) and (b) FT (in the nighttime) conditions throughout the sampling period.

Figure 4.2 shows temporal variations in the mass concentration of WSOC in comparison with those of sulfate, bromide, MSA, and 2-methyltetrol under the MBL and FT conditions during the entire period. These average concentrations of WSOC in the MBL are substantially larger than those previously observed (~60 ngC m^{-3}) at Amsterdam Island located in the Austral Sector of the southern IO (Sciare et al., 2009). Sciare et al. (2009) suggested that atmospheric dilution induced by the long-range transport of marine aerosols resulted in the lower concentrations of WSOC in their study, which may partly explain the difference in the concentration of WSOC between the current study and their report. The average concentration of WSOC is higher in MBL condition for both wet (306 ± 140 ngC m^{-3}) and dry (303 ± 109 ngC m^{-3}) seasons compared to FT conditions for both wet (91 ± 64 ngC m^{-3}) and dry (32 ± 68 ngC m^{-3}) seasons shown in **Table 4.1.**

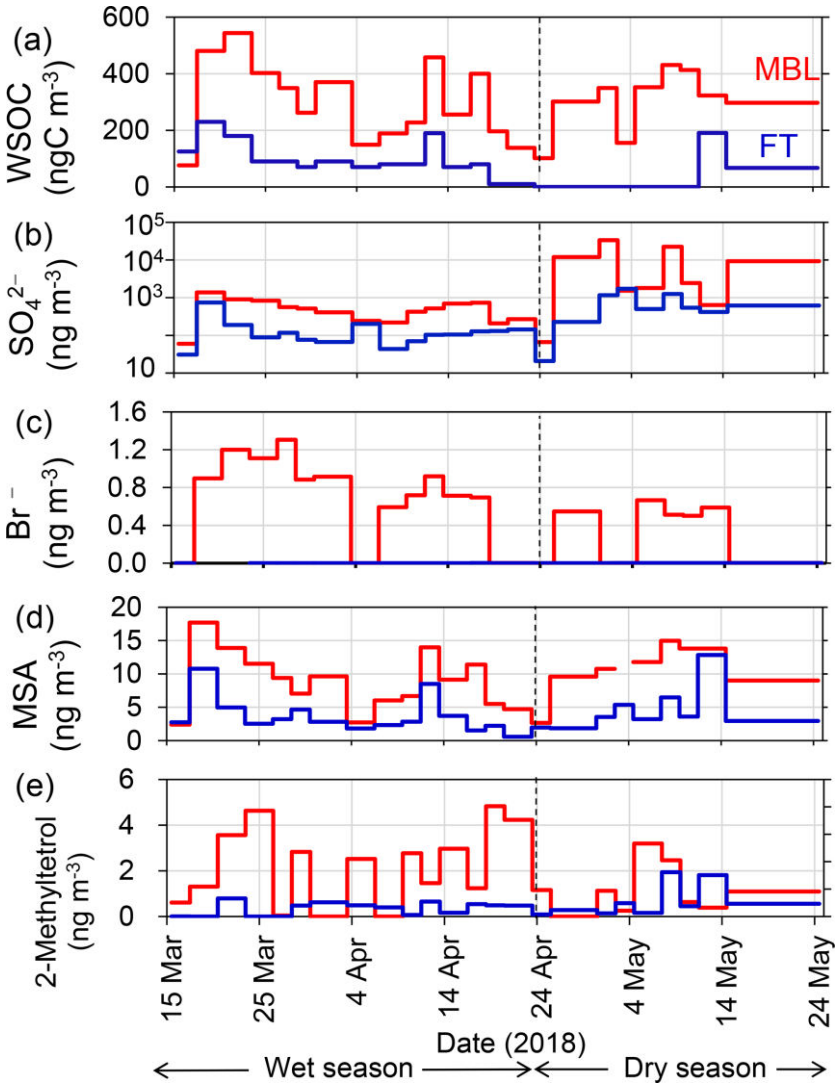

Figure 4.2 Time series of the mass concentrations of (a) WSOC, (b) sulfate, (c) bromide, (d) MSA, and (e) 2-methyltetrol under the MBL (red) and FT (blue) conditions.

Table 4.1 Average concentrations and ratios of the major parameters under the marine boundary layer (MBL; daytime) and free tropospheric (FT; nighttime) conditions at the Maïdo observatory during wet and dry seasons. The numbers in the parenthesis show the lower detection limit of mass concentration and the number of samples that showed values below the lower limit of detection (LOD) in each category. If the measured concentrations were below LOD, the concentrations were treated as zero when the averages and standard deviations were calculated.

	Wet season (Mar 15–Apr 23, 2018)		Dry season (Apr 24–May 24, 2018)	
	MBL (day) $n = 16$	FT (night) $n = 16$	MBL (day) $n = 8$	FT (night) $n = 8$
WSOC (ngC m^{-3})	306 ± 140 (2.7, 0)	91 ± 64 (3.1, 1)	303 ± 109 (2.7, 0)	32 ± 68 (3.1, 6)
$\delta^{13}C_{WSOC}$ (‰)	−23.2 ± 1.0	−23.5 ± 2.5	−24.3 ± 1.0	−25.0 ± 1.4
Sulfate (ng m^{-3})	511 ± 355 (1.0, 0)	141 ± 169 (1.1, 0)	10445 ± 11891 (1.0, 0)	804 ± 513 (1.1, 0)
Na^+ (ng m^{-3})	46.9 ± 160 (1.2, 3)	146 ± 492 (1.4, 1)	33.6 ± 32.6 (1.2, 0)	35.5 ± 34.6 (1.4, 0)
Br^- (ng m^{-3})	0.68 ± 0.40 (0.2, 2)	LOD (0.3, 16)	0.43 ± 0.27 (0.2, 2)	LOD (0.3, 8)
MSA (ng m^{-3})	8.39 ± 4.50 (0.4, 0)	3.57 ± 2.65 (0.5, 0)	11.7 ± 2.31 (0.4, 0)	4.96 ± 3.49 (0.5, 0)
2-Methyltetrol (ng m^{-3})	2.98 ± 3.20 (0.04, 1)	0.27 ± 0.23 (0.05, 4)	1.14 ± 1.13 (0.04, 1)	0.62 ± 0.60 (0.05, 0)
3-MBTCA (ng m^{-3})	0.35 ± 0.40 (0.01, 1)	0.02 ± 0.05 (0.01, 11)	0.24 ± 0.22 (0.01, 1)	0.09 ± 0.13 (0.01, 1)
Pinic acid (ng m^{-3})	0.14 ± 0.18 (0.01, 4)	0.03 ± 0.03 (0.01, 6)	0.06 ± 0.06 (0.01, 2)	0.05 ± 0.08 (0.01, 2)
Pinonic acid (ng m^{-3})	0.21 ± 0.15 (0.01, 2)	0.06 ± 0.06 (0.01, 2)	0.15 ± 0.15 (0.01, 1)	0.04 ± 0.03 (0.01, 1)

The extremely high sulfate concentrations observed both in the MBL (up to ~33000 ng m^{-3}) and in the FT (up to ~1700 ng m^{-3}) in the dry season (**Figures 4.2b**), are attributable to the eruption of Piton de la Fournaise volcano in the southeast of La Réunion, which started on April 27 and continued until the beginning of June, 2018. **(Figure 4.3)** Time series of sulfate concentration shows the drastic changes of the concentration level from wet season to dry season due to volcanic eruption. The air masses affected by the volcanic eruption in the southeast of the island were frequently transported to the observatory, where this transport pathway was explained by the strong trade wind which is commonly observed in the dry season. In contrast, no significant corresponding increase in the WSOC concentration during this period (**Figure 4.2a**) was observed, suggesting that the contribution of the volcanic eruption to the WSOC mass was insignificant.

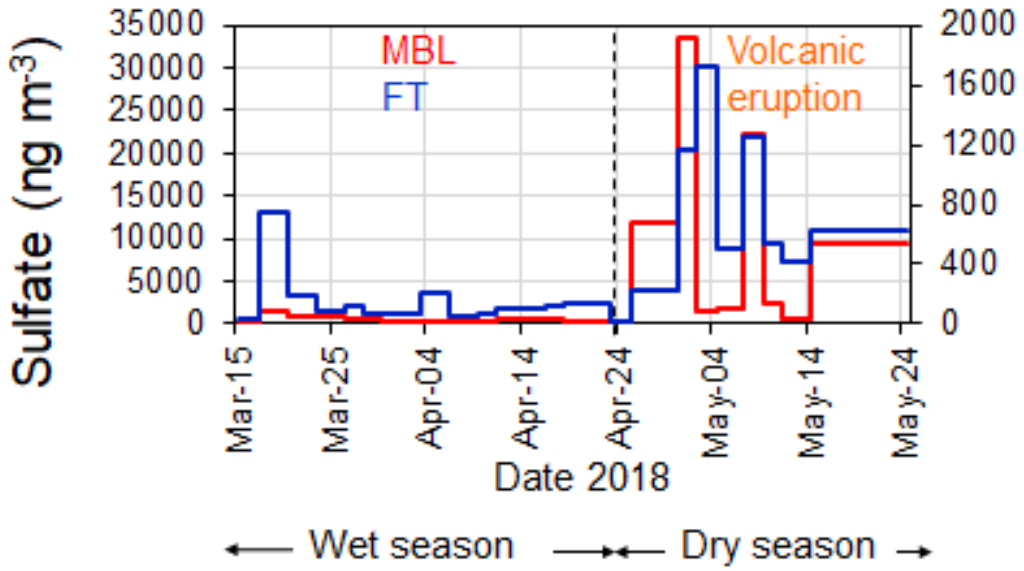

Figure 4.3 Time series of the sulfate concentration (a) MBL (in the daytime) and (b) FT (in the nighttime) conditions throughout the sampling period.

Bromide has been used as a tracer of marine emissions because its production is closely related to biological activity (Zhu et al.,2019). On the other hand, MSA is formed by the oxidation of dimethyl sulfide (DMS) emitted from the marine surface and used as a tracer of marine secondary production (Hodshire et al., 2019). Substantially larger concentrations of bromide and MSA in the MBL than in the FT were also observed (**Figure 4.2c** and **4.2d**). More active photochemical reactions promote the oxidation of precursors to form secondary aerosols during daytime (MBL) (Shen et. al., 2018). The average bromide concentration in the wet season was twice as large as that in the dry season (**Table 4.1**), reflecting higher biological productivity (Anbar et al., 1996; Hu et al., 2012; Zhu et al., 2019) in the wet season. Indeed, during the study period, marine primary productivity in the IO showed larger values in March, and decreased from March to May as discussed in Chapter 3.

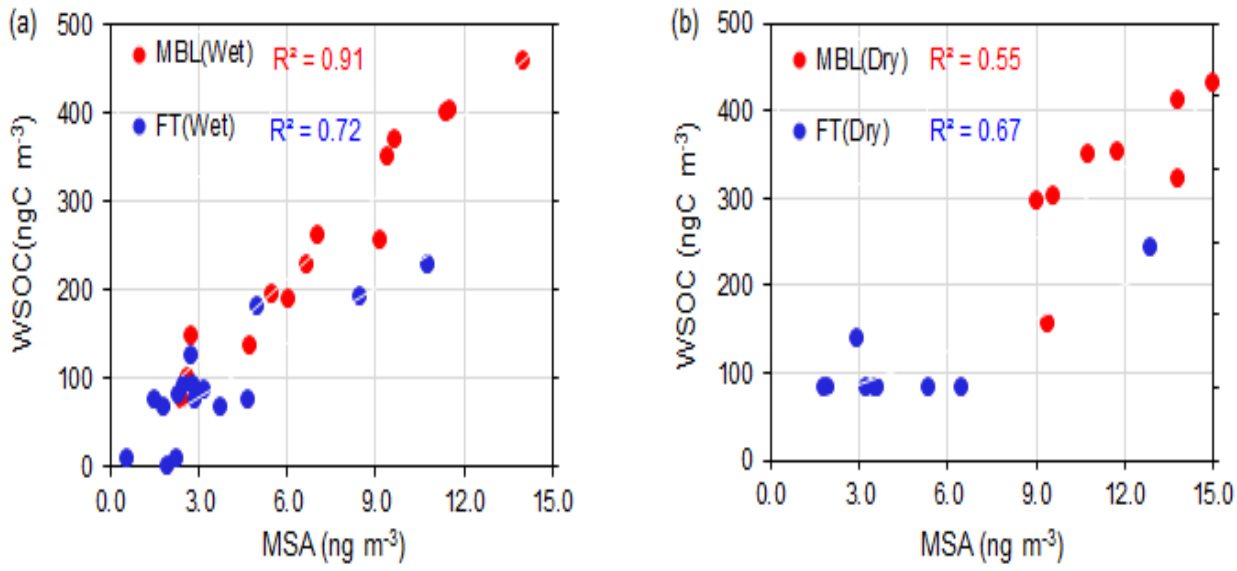

Figure 4.4 Correlation between WSOC and MSA for (a) wet season and (b) dry season under the MBL (red) and FT (blue) conditions.

The temporal variation in the concentration of MSA is similar to that of WSOC during the wet season for both MBL and FT with the R^2 of 0.91 and 0.72, respectively, ($p < 0.01$) (**Figure 4.4**), suggesting that the dominant source of WSOC is similar to that of MSA. The concentration of 2-methyltetrol, an oxidation product of isoprene, was typically higher in the MBL than in the FT in the wet season (**Figure 4.2e**), although their temporal variations are generally different from those of WSOC ($R^2 < 0.01$) with exceptions of a few samples. The contributions of terrestrial sources are further discussed in the following sections.

Figure 4.5 shows the temporal variation of the air pressure and the mass concentration of WSOC under the MBL and FT conditions during the wet and dry seasons. The air pressure varied on a time scale of about 10 days, which corresponded to the temporal variations of the concentrations of WSOC as well as the other parameters (**Figure 4.2**), particularly in the MBL. This indicates that the temporal variation of the mass concentration of aerosol on time scales of ~10 days shown in **Figure 4.2** can be partly explained by the synoptic-scale meteorology in the oceanic region as discussed in Chapter 3.

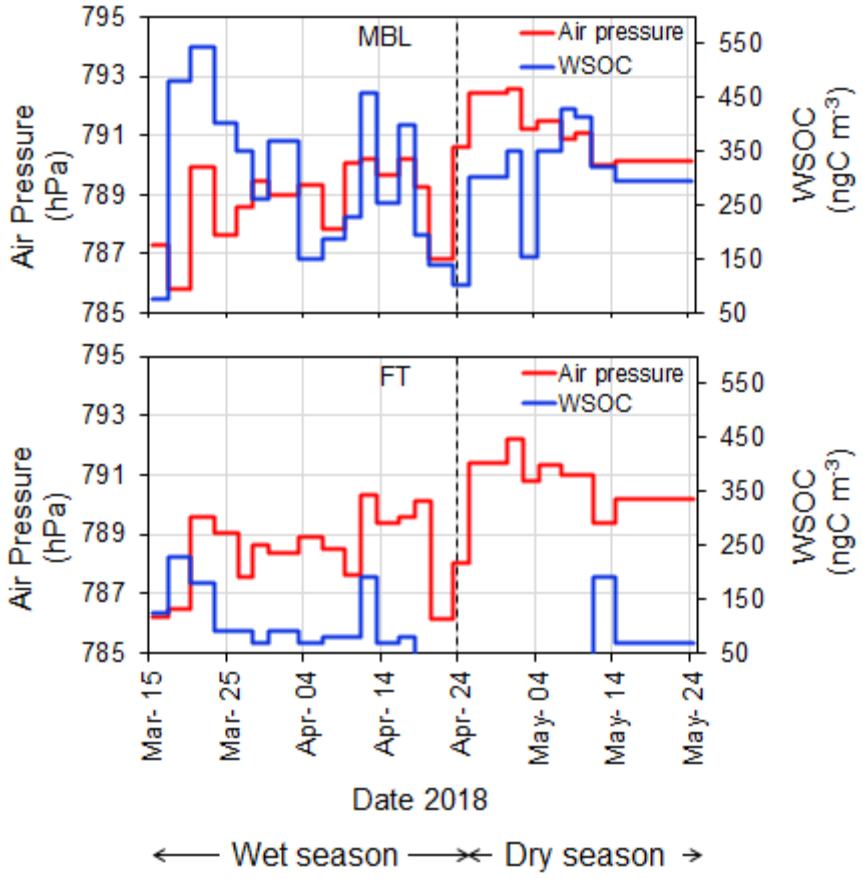

Figure 4.5 Temporal variation of air pressure in comparison with the aerosol concentrations of WSOC under MBL and FT conditions during wet and dry seasons.

4.3 Isotopic characterization of WSOC and FLEXPART backward trajectories

The isotopic composition of aerosol carbon has been used frequently to determine the contributions of marine and terrestrial sources to aerosol carbon mass found in the remote marine atmosphere (e.g., Cachier et al., 1986). In particular, the WSOC-specific stable carbon isotopic composition ($\delta^{13}C_{WSOC}$) provides robust tools for the source apportionment of aerosol WSOC in the marine atmosphere (e.g., Miyazaki et al., 2016). **Figure 4.6** shows the temporal variation in the $\delta^{13}C_{WSOC}$ value of the submicrometer aerosols during the entire period. Based on previous

studies (e.g., Cachier et al., 1986; Turekian et al., 2003), here we assume that $\delta^{13}C_{WSOC} > -24‰$ indicates that WSOC was primarily originated from marine sources, whereas $\delta^{13}C_{WSOC} < -24‰$ indicates WSOC mainly affected by terrestrial sources, with the uncertainty of ±1.0‰. In the wet season, 87% and 83% of the data in the MBL and the FT, respectively, showed the $\delta^{13}C_{WSOC}$ values larger than −24‰, with averages of −23.2 ± 1.0‰ (MBL) and −23.5 ± 2.5‰ (FT). While these average values with the uncertainty were close to −24‰, the larger concentrations of WSOC (e.g., > 300 ngC m^{-3} in MBL; **Figure 4.2a**) corresponded to a higher $\delta^{13}C_{WSOC}$ value (> −24‰). In particular, the larger concentrations of WSOC (e.g., > 300 ngC m^{-3} in MBL; **Figure 4.2a**) corresponded to a higher $\delta^{13}C_{WSOC}$ value(> −24‰). The results suggest that marine sources contributed significantly to the WSOC mass under both the MBL and FT conditions during the wet season. In contrast, the average $\delta^{13}C_{WSOC}$ value in the dry season were −24.4 ± 1.0‰ and −25.0 ± 1.4‰ in the MBL and FT, respectively, where 33% (MBL) and 33% (FT) of the data showed $\delta^{13}C_{WSOC} > -24‰$.

To estimate the relative contribution of marine and terrestrial OC sources to the observed WSOC, a mass balance equation (e.g., Turekian et al., 2003) was applied with the following equations:

$$\delta^{13}C_{WSOC} = F_{marine} \times \delta^{13}C_{marine} + F_{terrestrial} \times \delta^{13}C_{terrestrial}$$

where F_{marine} and $F_{terrestrial}$ are the fractions of marine and terrestrial carbon respectively, and $\delta^{13}C_{marine}$ and $\delta^{13}C_{terrestrial}$ are the reported $\delta^{13}C$ values for marine and terrestrial carbon, respectively. The $\delta^{13}C$ value is assumed to be −21.5 ± 1‰ for marine OC (Turekian et al., 2003; Miyazaki et al., 2010), and −28 ± 1‰ for terrestrial OC (e.g., Cachier et al., 1986). Here, we

applied these $\delta^{13}C$ values as end-members of marine and continental aerosols to calculate the relative contribution. Our calculations indicate that marine sources contributed by ~75% and ~71% in MBL and FT, respectively, during the wet season. The estimated contributions of marine sources are reduced to ~55% and ~46% in the MBL and in the FT, respectively, during the dry season, suggesting that the WSOC mass was attributed to both marine and terrestrial sources with similar fractional contributions in the MBL and FT during the dry season.

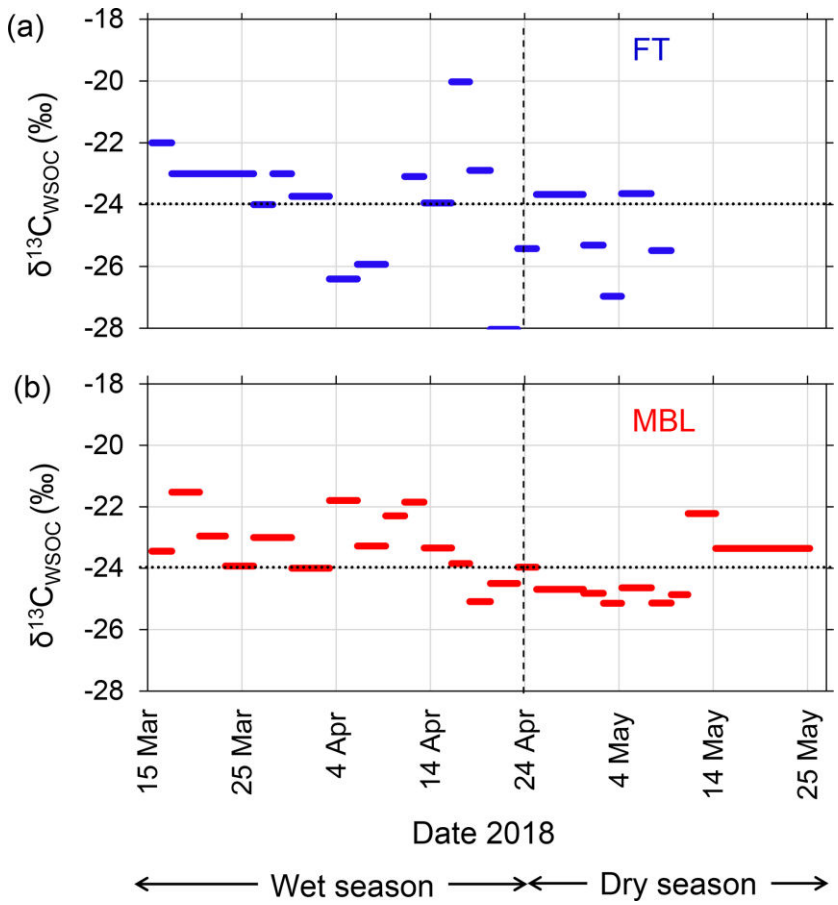

Figure 4.6 Time series of stable carbon isotope ratio of WSOC ($\delta^{13}C_{WSOC}$) under (a) FT and (b) MBL conditions during the entire sampling period. Dashed lines indicate the transition from wet to dry seasons. Dotted lines indicate the boundary of $\delta^{13}C_{WSOC}$ ranges distinguishing assumed marine (> −24‰) and terrestrial sources (< −24‰).

Figure 4.7 presents a representative ten-day back trajectory calculated by FLEXPART, which shows the surface contribution to the measured air mass at the Maïdo observatory. The calculated air parcels were initialized at the Maïdo observatory under the MBL and FT conditions in each seasonal category throughout the sampling periods. Overall, the air-mass flow pattern shown in the figure is controlled by Mascarene High, located over the southern IO, whose location shifts westward during the dry season (e.g., Mallet et al., 2018). The Lagrangian trajectory analysis showed that most air parcels in the wet season were transported over the southern Indian Ocean. This is consistent with the results of the isotopic analysis and suggested that the majority of submicrometer WSOC originated from the sea surface during the wet season. During the dry season, some portion of the trajectories passed over southern Africa in addition to the southern Indian Ocean, indicating some influence from the land surface in addition to the marine source. This is also consistent with the results from the isotopic analysis of WSOC, which suggest the influence of both land and the ocean surface.

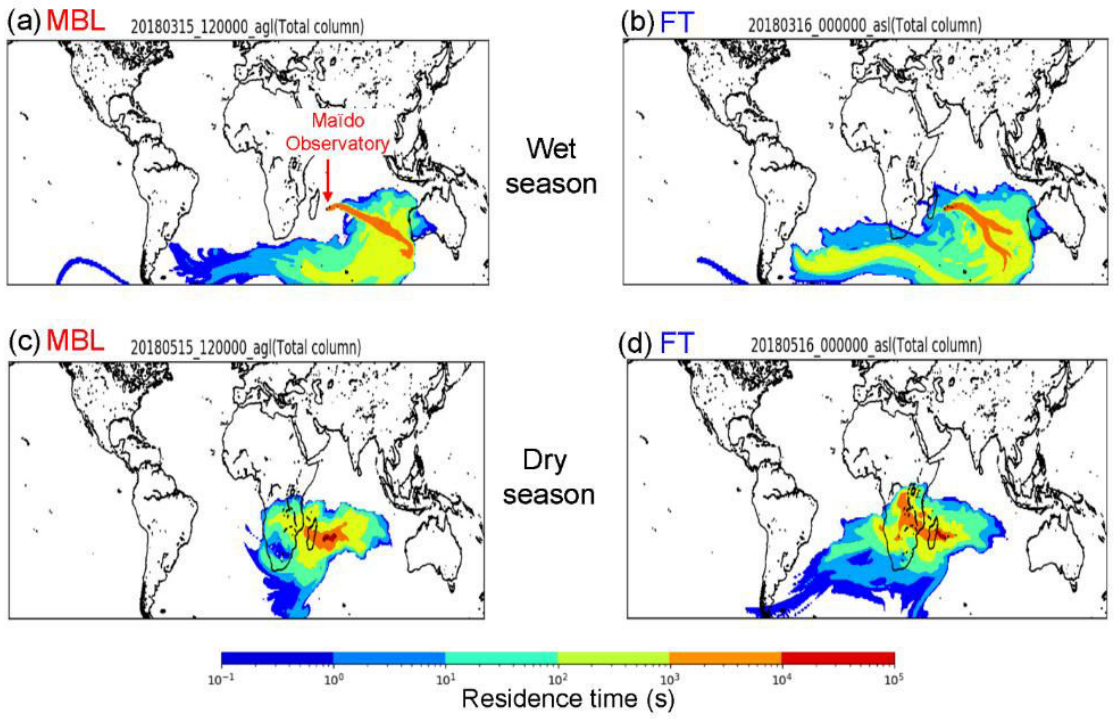

Figure 4.7 Representative source–receptor relationships for aerosols observed at the Maïdo observatory for ten-day periods starting at the time under the (a) MBL and (b) FT conditions during the wet season and (c) MBL and (d) FT during the dry season, which were calculated by FLEXPART. The color code represents the surface contribution to the measured air mass at the Maïdo observatory. Each color represents the degree of the surface contribution that varies by a factor of 10. For example, the orange color shows the surface contribution ten times larger than yellow.

4.4 Source apportionment of WSOC by positive matrix factorization

To further investigate the possible sources of the submicrometer WSOC under different conditions, a PMF analysis was performed as described in 2.6. PMF analysis illustrates each factor profile calculated by the PMF. The PMF resolved six interpretable factors, which were characterized by the enrichment of each tracer compound in a factor compared to the other factors. Factor 1 (F1) was characterized by the significant contribution of MSA (~50%). Consequently, it

is referred to here as “marine SOA.” In fact, previous cruise measurements showed that in the southern IO, the sea-to-air emission of DMS is more active than that of other oceanic regions (Sciare et al., 1999) and that DMS was the most abundant VOC measured in the atmosphere (Colomb et al., 2009). The oceanic regions mentioned in these previous studies overlap with the possible oceanic source region shown in **Figures 4.6a** and **4.6b**.

Factor 2 (F2) is characterized by sea salt components, such as sodium (66%) and magnesium (78%). Moreover, bromide also contributed significantly to F2, which is thus referred to here as “marine primary aerosols.” It is interesting that bromide also had a significant contribution to F1 (marine SOA). Bromide is expected to be recycled rather quickly via the gas phase and redistributed among all types of aerosols on time scales of minutes to a few hours after emission (e.g., Zhu et al., 2019). Therefore, primary bromide, which is emitted with sodium as a part of sea spray aerosols, is expected to appear in F1 (marine SOA). Because Factor 3 (F3) is dominated by sulfate (68%), it is defined as “the sulfate-dominated” source. Factor 4 (F4) is characterized by the dominant contributions of 2-methyltetrol and *n*-nonacosan-10-ol. Miyazaki et al. (2019) identified *n*-nonacosan-10-ol in forest aerosols, suggesting that they mainly originated from plant waxes and could be a tracer of primary biological aerosol particles. Consequently, F4 is referred to here as “terrestrial biogenic sources.” Although Factor 5 (F5) was difficult to attribute to a specific source, given the possibility that nitrate is associated with terrestrial sources with smaller contributions of marine tracers, F5 was labeled here as “terrestrial sources (Anthropogenic + Biogenic).” Similarly, Factor 6 (F6) is dominated by ammonium (50%) with a mixture of tracers of marine and terrestrial sources. F6 is referred to as “the mixture of marine and terrestrial sources” as a possible source category of WSOC.

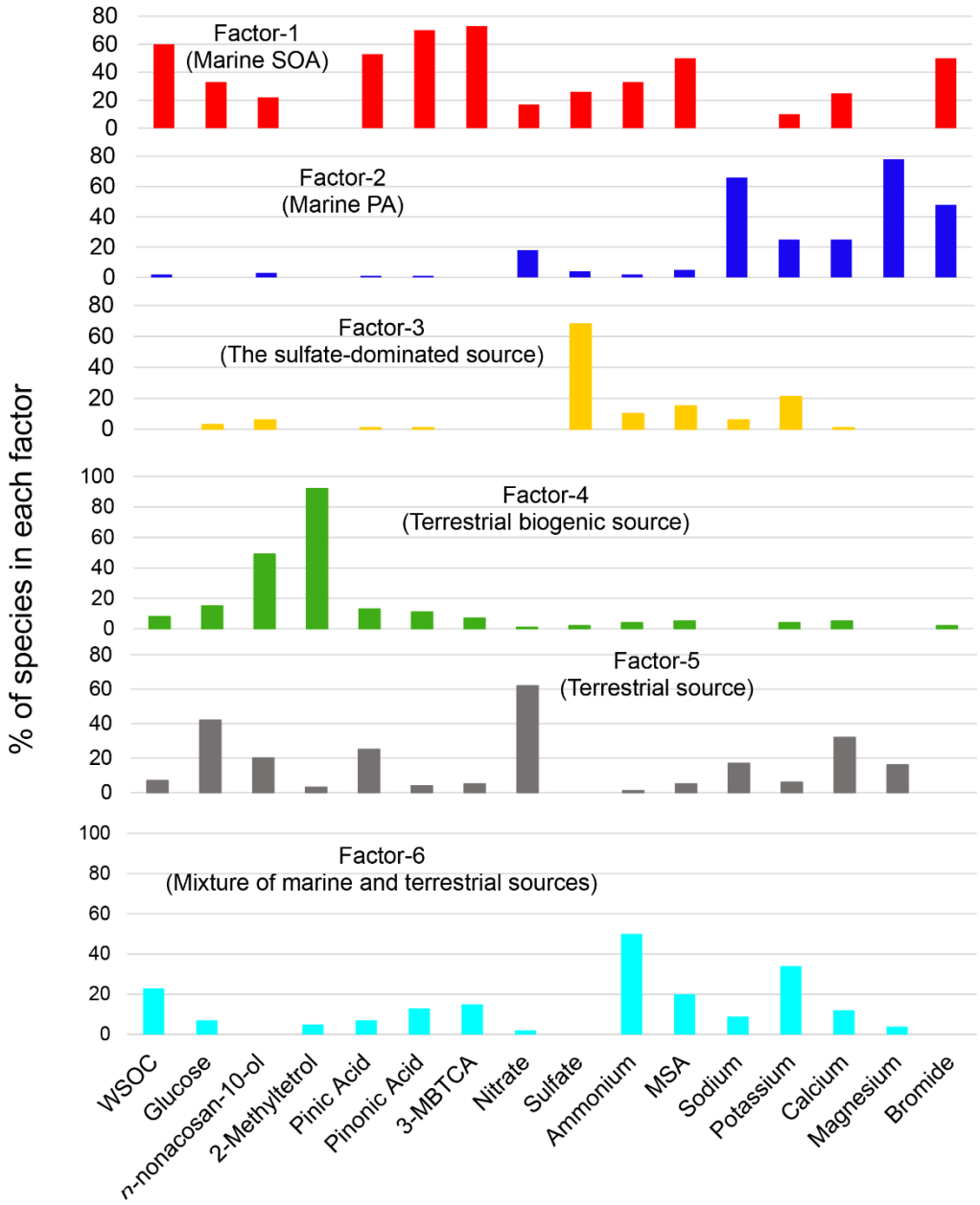

Figure 4.8 Six factor profiles for the entire campaign derived from PMF analysis. The percentage of chemical species in each factor is shown.

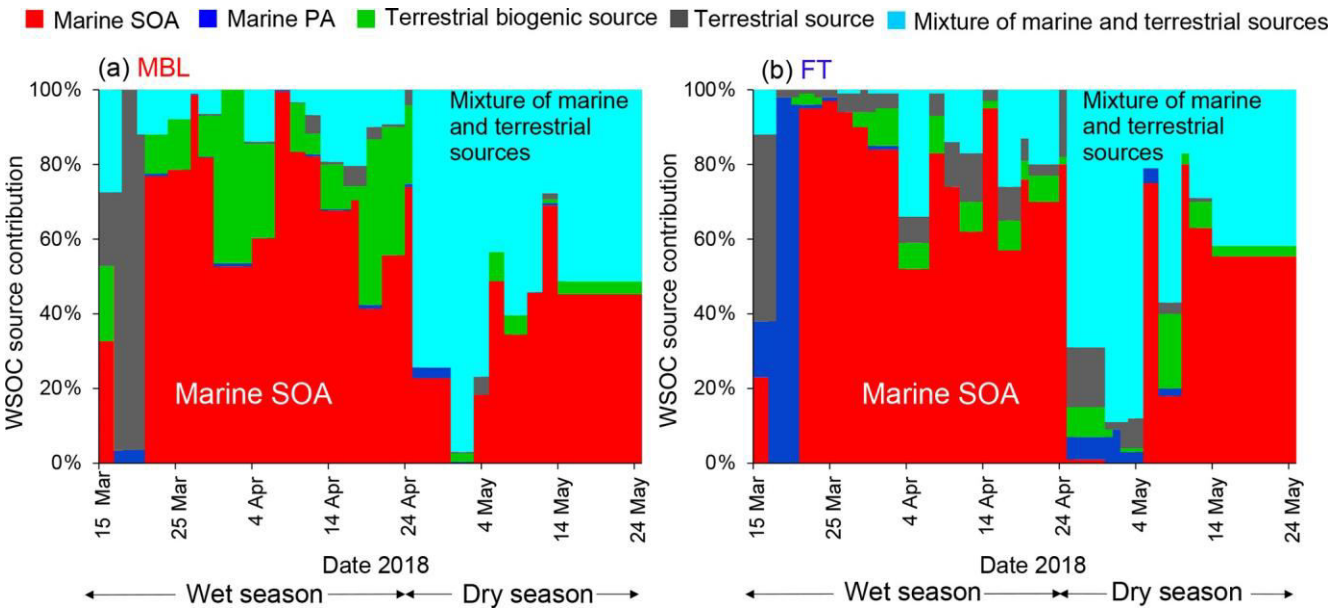

Figure 4.9 Time series of the contributions of each PMF-derived factor to the WSOC mass concentration under the (a) MBL and (b) FT conditions.

Figure 4.9 shows the time series of the mass contributions of the individual identified factors to the WSOC mass concentrations in the MBL and FT. The average contributions of each PMF-derived factor to the WSOC mass are also summarized in **Figure 4.8**. A distinct temporal shift of the dominant source of WSOC was apparent from the wet season to the dry season in both the MBL (**Figure 4.10a**) and FT (**Figure 4.10b**). On average, marine SOA dominantly contributed to the WSOC mass (~66% – 70%) in both the MBL and FT during the wet season. Marine SOA and mixtures of marine/terrestrial sources had similar contributions to WSOC in MBL and FT during the dry season (**Figure 4.10a** and **4.10b**). On average, terrestrial biogenic sources, which are mainly based on the contribution of 2-methyltetrol, accounted for 16% of the WSOC mass in the MBL during the wet season. Specifically, the contribution of terrestrial biogenic sources was more

than 40% of the WSOC mass around April 1 and April 19 in the MBL. Previous cruise measurements of VOCs suggested oceanic emissions of isoprene in the southern IO during austral summer (December) (e.g., Colomb et al., 2009). However, the data exhibiting large contributions of terrestrial biogenic sources mentioned above showed a lower $\delta^{13}C_{WSOC} < -24‰$ (**Figure 4.6b**), supporting the validity of the definition of the PMF factor as terrestrial biogenic sources rather than marine biogenic origin. These biogenic sources are attributable to local terrestrial biogenic emissions of VOCs on La Réunion Island, followed by the upward transport along the slope of the island, particularly in the daytime (Verreyken et al., 2020). It is noted that F1 also had large contributions of oxidation products of α-pinene (i.e., pinic acid, pinonic acid, and 3-MBTCA; **Figure 4.8**). The regression analysis showed that R^2 of WSOC with pinic acid, pinonic acid, and 3-MBTCA were 0.53 ($p < 0.01$), 0.27 ($p < 0.01$), and 0.26 ($p < 0.01$), respectively. These results are also attributable to local terrestrial biogenic emissions of VOCs during the transport from the ocean to the observatory. However, the dominance of marine SOA as a source of WSOC in the wet season (**Figure 4.9**) is consistent with the $\delta^{13}C_{WSOC}$ values, supporting the validity of the definition of F1 and that the contribution of α-pinene SOA from local biogenic sources to the WSOC mass was small in this case.

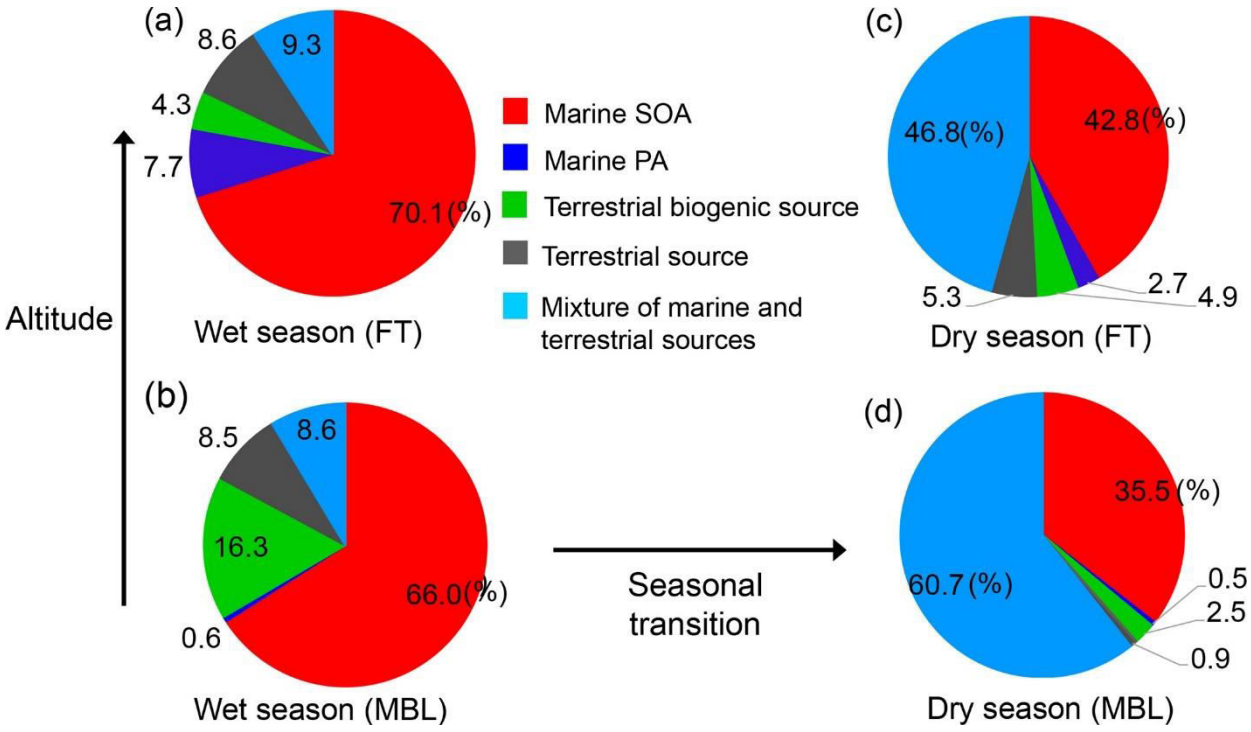

Figure 4.10 Average contribution of each PMF-derived factor to the WSOC mass concentration during the wet season ((a) and (b)) and dry season ((c) and (d)). The pie charts are further classified under (a, c) FT and (b, d) MBL conditions.

Mixtures of marine and terrestrial sources significantly contributed to the WSOC mass during the dry season, where they accounted for 61% and 47% of the WSOC mass in the MBL and FT, respectively (**Figure 4.10c** and **4.10d**). These results point to the importance of marine SOA up the FT during the wet season, which is attributed to the high oceanic productivity in this region (Zhou et al., 2019), as well as to significant vertical transport of air during this season. It is noted that a few samples showed some contributions of terrestrial sources mainly explained by nitrate (**Figure 4.8**), which was attributable to the effect of local anthropogenic sources. In fact, two tropical cyclone events (March 13–21 and April 18–26) can explain the increased concentrations of nitrate in those limited samples (**Figure 4.1**), when air masses on a local scale were vertically

transported rapidly to the sampling site. However, our measurement of the $\delta^{13}C_{WSOC}$ values suggests that the majority of the observed WSOC originated from marine sources particularly during wet seasons. Therefore, possible contributions of local contamination to the WSOC concentrations are likely minor in our study.

It is also noted that the average contribution of marine primary aerosols to the WSOC mass was higher in FT than in the MBL (**Figure 4.10**). This was attributable to the two samples that showed dominant or higher contributions of marine primary aerosol to the WSOC mass in FT at the beginning of both wet and dry seasons. These can be explained by the two cyclone events mentioned above when marine primary aerosols were rapidly transported to FT. Although the source apportionment of WSOC only by PMF has a limitation with a limited number of samples in the current study, the overall result is supported by the measurements of the $\delta^{13}C_{WSOC}$ values as well as the results of FLEXPART, which are consistent with the output of PMF.

4.5 Secondary formation of marine-derived WSOC and its implications

It is possible that the aging of marine primary organic aerosols (POA) and subsequent formation of more oxidized OA significantly contributed to the observed WSOC mass. Mallet et al. (2018) presented an 8-year satellite dataset of the distribution and variability of marine aerosols over the southern IO, which included the current aerosol sampling site. They suggested that aerosols are mainly confined below 2 km above sea level and are dominated by sea salt over the southern IO. However, the mass fraction of sea salt in the submicrometer particles observed at the Maïdo observatory (2,160 m a.s.l) was insignificant, which resulted in a significantly lower contribution from marine primary aerosol (PA) (**Figures 4.9** and **4.10**). Therefore, the current

results indicate that the aging of marine POA is insignificant, and the contribution of VOC oxidation from the sea surface to the WSOC mass up to the lower FT is likely more important.

Brüggemann et al. (2018) indicated that, especially in tropical regions with low POA concentrations, SOA from oxidation of photochemically produced VOCs contributes up to 60% of additional OA mass, such as over the IO, by modeling. In summary, the results of the current study highlight the importance of marine biogenic SOA up to the lower FT, a process missing in climate models. Current models typically consider only marine POA (i.e., SSA) from the sea surface to represent the OA burden in tropical "pristine" oceanic regions (e.g., Gantt et al., 2015). The impacts of marine SOA up to FT aerosols lead to changes in the microphysical and optical properties of aerosol particles. Model calculations (Zhu et al., 2017) suggested that the contribution of SOA to radiative forcing will increase substantially in the future even if the increase of SOA burden is slight and without considering the combined effects of changes in marine SOA. The current results may have important implications for understanding the climate effects of aerosols in these oceanic regions.

4.6 Conclusions

In this chapter, the origins of WSOC in submicrometer aerosols were investigated based on continuous ambient aerosol sampling at the Maïdo observatory in La Réunion in the southwest Indian Ocean. OM was the dominant component of the submicrometer water-soluble aerosol (~46 ± 10%) in the MBL during the wet season, whereas sulfate dominated (~77 ± 19%) during the dry season. The estimation using the stable carbon isotope ratios of WSOC showed that, on average, for the wet season, marine sources accounted for ~75% and ~71% of the WSOC mass in MBL and

FT, respectively. Conversely, marine sources contributed ~55% and ~46% in MBL and FT, respectively, of the WSOC mass during the dry season, suggesting that the WSOC mass was attributed to both marine and terrestrial sources in the MBL and FT during that season. The significant seasonal difference in the dominant source of WSOC between the two seasons was also supported by Lagrangian trajectory analysis.

The PMF analysis suggested that marine SOA was a dominant contributor to the observed WSOC mass (~70%) during the wet season, whereas mixtures of marine and terrestrial sources accounted for 61% and 47% of the WSOC mass in the MBL and FT, respectively. Overall, this study demonstrates that emissions of biogenic VOCs from the ocean surface followed by the formation of SOA are likely important up into the FT during the wet season when marine biological activity and vertical transport are more significant. These characteristics may affect subsequent cloud formation as well as the direct radiative forcing over this oceanic region.

References

Anbar, A. D., Yung, Y. L. and Chavez, F. P.: Methyl bromide: Ocean sources, ocean sinks, and climate sensitivity, Global Biogeochem. Cycles, 10, 175–190, https://doi.org/10.1029/95GB02743, 1996.

Brüggemann, M., Hayeck, N. and George, C.: Interfacial photochemistry at the ocean surface is a global source of organic vapors and aerosols, Nat. Commun., 9, 1–8, https://doi.org/10.1038/s41467-018-04528-7, 2018.

Cachier, H., Buat-Menard, P., Fontugne, M. and Chesselet, R.: Long-range transport of continentally-derived particulate carbon in the marine atmosphere: Evidence from stable carbon isotope studies, Tellus B, 38, 161–177, https://doi.org/10.3402/tellusb.v38i3-4.15125, 1986.

Colomb, A., Gros, V., Alvain, Ś., Sarda-Esteve, R., Bonsang, B., Moulin, C., Klpfel, T. and Williams, J.: Variation of atmospheric volatile organic compounds over the Southern Indian Ocean (3049°S), Environ. Chem., 6, 70–82, https://doi.org/10.1071/EN08072, 2009.

Gantt, B., Glotfelty, T., Meskhidze, N. and Zhang, Y.: Simulating the impacts of marine organic emissions on global atmospheric chemistry and aerosols using an online-coupled meteorology and chemistry model, Atmos. Clim. Sci., 5, 266-274, https://doi. 10.4236/acs.2015.53020, 2015.

Hodshire, A. L., Campuzano-Jost, P., Kodros, J. K., Croft, B., Nault, B. A., Schroder, J. C., Jimenez, J. L. and Pierce, J. R.: The potential role of methanesulfonic acid (MSA) in aerosol formation and growth and the associated radiative forcings, Atmos. Chem. Phys., 19, 3137–3160, doi:10.5194/acp-19-3137-2019, 2019.

Hu, L., Yvon-Lewis, S., Liu, Y. and Bianchi, T. S.: The ocean in near equilibrium with atmospheric methyl bromide, Global Biogeochem. Cycles, 26, 1–11, https://doi.org/10.1029/2011GB004272, 2012.

Mallet, P. É., Pujol, O., Brioude, J., Evan, S. and Jensen, A.: Marine aerosol distribution and variability over the pristine Southern Indian Ocean, Atmos. Environ., 182, 17–30, https://doi.org/10.1016/j.atmosenv.2018.03.016, 2018.

Miyazaki, Y., Kawamura, K. and Sawano, M.: Size distributions of organic nitrogen and carbon in remote marine aerosols: Evidence of marine biological origin based on their isotopic ratios, Geophys. Res. Lett., 37, L06803, https://doi.org/10.1029/2010GL042483, 2010.

Miyazaki, Y., Coburn, S., Ono, K., Ho, D. T., Pierce, R. B., Kawamura, K. and Volkamer, R.: Contribution of dissolved organic matter to submicron water-soluble organic aerosols in the marine boundary layer over the eastern equatorial Pacific, Atmos. Chem. Phys., 16, 7695–7707, https://doi.org/10.5194/acp-16-7695-2016, 2016.

Miyazaki, Y., Gowda, D., Tachibana, E., Takahashi, Y. and Hiura, T.: Identification of secondary fatty alcohols in atmospheric aerosols in temperate forests, Biogeosciences, 16, 2181–2188, https://doi.org/10.5194/bg-16-2181-2019, 2019.

Sciare, J., Mihalopoulos, N. and Nguyen, B. C.: Summertime seawater concentrations of dimethylsulfide in the western Indian Ocean: Reconciliation of fluxes and spatial variability with long-term atmospheric observations, J. Atmos. Chem., 32, 357–373, https://doi.org/10.1023/A:1006132001945, 1999.

Sciare, J., Favez, O., Sarda-Estève, R., Oikonomou, K., Cachier, H. and Kazan, V.: Long term observations of carbonaceous aerosols in the Austral Ocean atmosphere: Evidence of a

biogenic marine organic source, J. Geophys. Res., 114, D15302, https://doi.org/10.1029/2009JD011998, 2009.

Shen, Z., Cao, J., Zhang, L., Liu, L., Zhang, Q., Li, J., Han, Y., Zhu, C., Zhao, Z. and Liu, S.: Day-night differences and seasonal variations of chemical species in PM_{10} over Xi'an, Northwest China, Environ. Sci. Pollut. Res., 21, 3697–3705, https://doi.org/10.1007/s11356-013-2352-z, 2014.

Turekian, V. C., Macko, S. A. and Keene, W. C.: Concentrations, isotopic compositions, and sources of size-resolved, particulate organic carbon and oxalate in near-surface marine air at Bermuda during spring, J. Geophys. Res.-Atmos., 108, 4157, https://doi.org/10.1029/2002jd002053, 2003.

Verreyken, B., Amelynck, C., Brioude, J., Muller, J. F., Schoon, N., Kumps, N., Colomb, A., Metzger, J. M., Lee, C. F., Koenig, T. K., Volkamer, R. and Stavrakou, T.: Characterisation of African biomass burning plumes and impacts on the atmospheric composition over the south-west Indian Ocean, Atmos. Chem. Phys., 20, 14821–14845, https://doi.org/10.5194/acp-20-14821-2020, 2020.

Zhou, S., Collier, S., Jaffe, D. A. and Zhang, Q.: Free tropospheric aerosols at the Mt. Bachelor Observatory: more oxidized and higher sulfate content compared to boundary layer aerosols, Atmos. Chem. Phys., 19, 1571–1585, https://doi.org/10.5194/acp-19-1571-2019, 2019.

Zhu, J., Penner, J. E., Lin, G., Zhou, C., Xu, L. and Zhuang, B.: Mechanism of SOA formation determines magnitude of radiative effects, Pr. Natl. Acad. Sci. U. S. A., 114, 12685–12690, https://doi.org/10.1073/pnas.1712273114, 2017.

Zhu, L., Jacob, D.J., Eastham, S.D., Sulprizio, M.P., Wang, X., Sherwen, T., Evans, M.J., Chen, Q., Alexander, B., Koenig, T.K., Volkamer, R., Huey, L. G., Le Breton, M., Bannan, T.J., and

Percival, C.J: Effect of sea-salt aerosol on tropospheric bromine chemistry, Atmos. Chem. Phys., 19, 6497-6507, https://doi.org/10.5194/acp-19-6497-2019.

Chapter 5. General Conclusions

In this study, the origins of WSOC in submicrometer aerosols were investigated based on continuous ambient aerosol sampling at the Maïdo observatory in La Réunion in the southwest Indian Ocean from March to May 2018. The observed levels of the water vapor mixing ratio and their seasonal changes confirm that the observatory was located in the MBL during the daytime, whereas it was in the FT at night. The wet season is characterized by higher marine primary productivity and atmospheric relative humidity than in the dry season. Moreover, synoptic-scale meteorology is more evident, which accompanies more active vertical transport of air from the ocean surface. In MBL, the OC concentrations during the wet season were generally higher than those during the dry season, which likely reflect higher marine primary productivity and more active vertical transport of air from the ocean surface. The temporal trends of OC and WSOC suggest that the water-soluble fraction of OC was an important factor controlling the total organic matter in the submicrometer aerosols during the wet season.

Organic matter was the dominant component of the submicrometer water-soluble aerosols (~46 ± 10%) in the MBL during the wet season, whereas sulfate dominated (~77 ± 19%) during the dry season. Estimation by using the stable carbon isotope ratios of WSOC showed that, on average, for the wet season, marine sources accounted for ~74% and ~69% of the WSOC mass in MBL and FT, respectively. Conversely, marine sources contributed ~55% and ~46% in MBL and FT, respectively, of the WSOC mass during the dry season, suggesting that the WSOC mass was attributed to both marine and terrestrial sources in the MBL and FT during that season. The

significant seasonal difference in the dominant source of WSOC between the two seasons was also supported by Lagrangian trajectory analysis.

The PMF analysis suggested that marine SOA was a dominant contributor to the observed WSOC mass (~70%) during the wet season. Meanwhile, mixtures of marine and terrestrial sources accounted for 61% and 47% of the WSOC mass in the MBL and FT, respectively. The results of the PMF were generally consistent with the stable carbon isotope ratios and the trajectory analysis.

The implication of this study is summarized in **Figure 5.1**. Overall, this study suggested that emissions of biogenic VOCs from the ocean surface followed by the formation of SOA are likely important up into the FT during the wet season, when marine biological activity and vertical transport are more significant. The formation of marine SOA is a process generally missing in current climate models, which leads to large uncertainties in quantitative outputs by such climate models. Current models typically consider only marine POA (i.e., SSA) from the sea surface to represent the OA burden in tropical "pristine" oceanic regions. The impacts of marine SOA up to FT aerosols lead to changes in the microphysical and optical properties of aerosol particles. The current results may have important implications for understanding the role of marine SOA on the climate effects of aerosols in these oceanic regions.

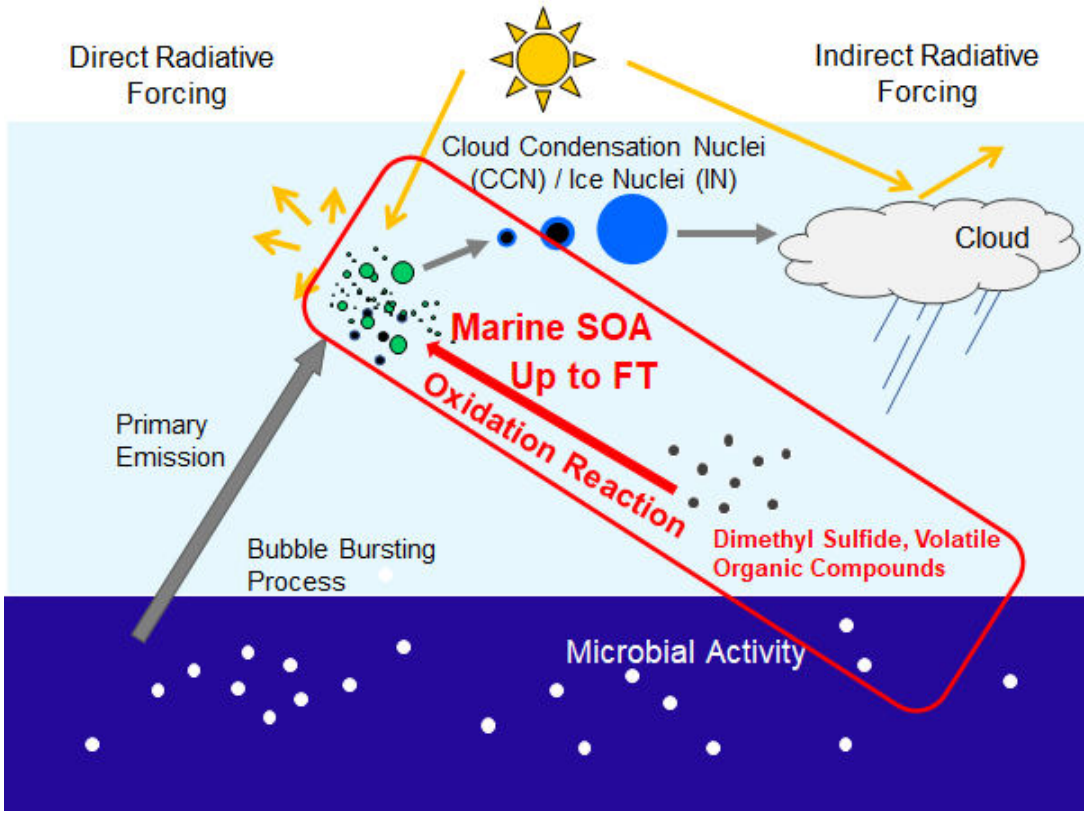

Figure 5.1 Schematic of the importance of the formation of marine SOA up to the lower free troposphere.